Battery Health Estimation in Electric Vehicles

VERENA KLASS

Doctoral Thesis, 2015
KTH Royal Institute of Technology
School of Chemical Science and Engineering
Department of Chemical Engineering and Technology
Applied Electrochemistry
SE-100 44 Stockholm, Sweden

TRITA CHE REPORT 2015:45
ISSN 1645-1081
ISBN 978-91-7595-671-8

Akademisk avhandling som med tillstånd av KTH i Stockholm framläggs till offentlig granskning för avläggande av teknisk doktorsexamen 9 oktober kl. 9.30 i Kollegiesalen, KTH, Brinellvägen 8, Stockholm.

”Obi, aufi, obi, aufi...”

When skiing

Abstract

For the broad commercial success of electric vehicles (EVs), it is essential to deeply understand how batteries behave in this challenging application. This thesis has therefore been focused on studying automotive lithium-ion batteries in respect of their performance under EV operation. Particularly, the need for simple methods estimating the state-of-health (SOH) of batteries during EV operation has been addressed in order to ensure safe, reliable, and cost-effective EV operation.

Within the scope of this thesis, a method has been developed that can estimate the SOH indicators capacity and internal resistance. The method is solely based on signals that are available on-board during ordinary EV operation such as the measured current, voltage, temperature, and the battery management system's state-of-charge estimate. The approach is based on data-driven battery models (support vector machines (SVM) or system identification) and virtual tests in correspondence to standard performance tests as established in laboratory testing for capacity and resistance determination.

The proposed method has been demonstrated for battery data collected in field tests and has also been verified in laboratory. After a first proof-of-concept of the method idea with battery pack data from a plug-in hybrid electric vehicle (PHEV) field test, the method was improved with the help of a laboratory study where battery electric vehicle (BEV) operation of a battery cell was emulated under controlled conditions providing a thorough validation possibility. Precise partial capacity and instantaneous resistance estimations could be derived and an accurate diffusion resistance estimation was achieved by including a current history variable in the SVM-based model. The dynamic system identification battery model gave precise total resistance estimates as well. The SOH estimation method was also applied to a data set from emulated hybrid electric vehicle (HEV) operation of a battery cell on board a heavy-duty vehicle, where on-board standard test validation revealed accurate dynamic voltage estimation performance of the applied model even during high-current situations. In order to exhibit the method's intended implementation, up-to-date SOH indicators have been estimated from driving data during a one-year time period.

Keywords

Lithium-ion battery, state-of-health, electric vehicle, support vector machine, resistance, capacity

Sammanfattning

För ett brett kommersiellt genomslag av elfordon är det viktigt att ordentligt förstå hur batterier beter sig i detta utmanande användningsområde. Doktorsarbetet har därför fokuserats på att studera prestandan hos litiumjonbatterier som används i elfordon. För att kunna garantera en säker, pålitlig och kostnadseffektiv användning har framförallt behovet av enkla metoder för uppskattning av batteriers hälsotillstånd ombord på elfordon adresserats.

Inom ramen för denna avhandling har en metod utvecklats som kan uppskatta hälsotillståndsindikatorerna kapacitet och inre resistans. Metoden baseras på signaler som är tillgängliga ombord på elfordon: den uppmätta strömmen, spänningen, temperaturen och laddningstillståndet uppskattat av batteriövervakningssystemet. Som angreppssätt har datadrivna batterimodeller (stödvektormaskin (SVM) eller systemidentifikation) valts. För att göra uppskattningar av kapacitet och resistanser har virtuella tester, motsvarande redan i laboratorier etablerade standardiserade prestandatester använts.

Metoden för att uppskatta hälsotillstånd har tillämpats på batteridata som samlats in under fälttest och har också verifierats med laboratorietester. Efter en första utvärdering av konceptet på batteripaketsdata från ett laddhybridtest i fält har metoden förbättrats genom en laboratoriestudie. Där har rena elfordonsanvändningen av en battericell emulerats under kontrollerade förhållanden, vilket gav möjligheten till ordentlig validering. Genom att en strömhistorievariabel inkluderades i den SVM-baserade modellen har den partiella kapaciteten, den momentana resistansen och diffusionsresistansen noggrant uppskattats. Även den dynamiska systemidentifikationsmodellen gav precisa uppskattningar av den totala resistansen. Metoden för att uppskatta hälsotillstånd har också tillämpats på data från emulerad hybridfordonsanvändning av en battericell ombord på ett tungt fordon. Standardtestvalideringen ombord visade en noggrann uppskattning av den dynamiska spänningen genom den använda modellen, även i situationer där hög ström applicerades. För att visa metodens tänkta implementering, har aktuella hälsotillståndsindikatorer uppskattats från körningsdata under en ettårsperiod.

List of appended papers

Paper I

Evaluating real-life performance of lithium-ion battery packs in electric vehicles

Verena Klass, Mårten Behm, Göran Lindbergh

Journal of The Electrochemical Society **159** (2012), A1856-A1860

Paper II

A support vector machine-based state-of-health estimation method for lithium-ion batteries under electric vehicle operation

Verena Klass, Mårten Behm, Göran Lindbergh

Journal of Power Sources **270** (2014), 262-272

Paper III

Capturing lithium-ion battery dynamics with support vector machine-based battery model

Verena Klass, Mårten Behm, Göran Lindbergh

Journal of Power Sources **298** (2015), 92-101

Paper IV

Dynamical lithium-ion battery model identification using electric vehicle operating data for resistance estimation

Verena Klass, Giuseppe Giordano, Mårten Behm, Göran Lindbergh, Jonas Sjöberg

Manuscript submitted to Journal of Power Sources

Paper V

State-of-health estimation of lithium-ion battery under emulated HEV operation on board heavy-duty truck

Verena Klass, Pontus Svens, Mårten Behm, Göran Lindbergh

Manuscript submitted to Applied Energy

Paper IV and V are the result of collaborations. The modeling and part of the writing in Paper IV was performed by Giuseppe Giordano. In Paper V, Pontus Svens collected the studied data and participated in the writing.

The following publications are not appended to this thesis:

Evaluating real-life performance of lithium-ion battery packs in electric vehicles

Verena Klass, Mårten Behm, Göran Lindbergh

ECS Transactions **41** (2012) 1-11

Li-ion battery performance in electric vehicles

Verena Klass, Mårten Behm, Göran Lindbergh

AABC 2010 - Advanced Automotive Battery Conference (2010) 45-48

Abbreviations

ARX	Autoregressive exogenous model
BEV	Battery electric vehicle
BMS	Battery management system
BOL	Beginning-of-life
CAN	Controller area network
CPU	Central processing unit
EV	Electric vehicle
HEV	Hybrid electric vehicle
LCO	Lithium cobalt oxide
LMO	Lithium manganese oxide
LTO	Lithium titanium oxide
NMC	Lithium nickel manganese cobalt oxide
OCV	Open circuit voltage
PHEV	Plug-in hybrid electric vehicle
RE	Relative error
RMSPE	Root-mean square percentage error
SOC	State-of-charge
SOH	State-of-health
SV	Support vector
SVM	Support vector machine
VE	Voltage error

Contents

Introduction

The vision of electrified transport is on the way to become reality. Most vehicle manufacturers have started selling electric vehicles (EVs)* and many cities strive to become sustainable and fossil fuel-free [1–8]. In Sweden, numerous demonstration activities have been initiated e.g. electrified buses in Stockholm and Gothenburg anticipating the full commercialization of electric vehicles in the near future [9,10].

From the point of view of sustainable cities, electrification of vehicles is desired for a number of reasons. All-electric vehicles are free from local emissions contributing to a better air quality and helping to meet emission regulations. In combination with a renewable energy generation from e.g. solar, wind, or hydro power, an overall emission reduction or even elimination can be achieved. In contrast to combustion-engine driven vehicles, all-electric vehicles are quiet opening up for new application areas like nighttime distribution and low-noise waste collection. Further benefits of electric vehicles in comparison to combustion-engine driven cars are the higher energy efficiency of the electric drive train, regeneration of braking energy, and fuel independency. For EV users, the low operating and maintenance costs are also an important advantage [11,12].

For the vision of electrified transport to be successfully realized, amongst other transitions, electric vehicles have to be sustainably introduced on a broad scale. As a prerequisite, EVs have to be safe, reliable, and cost-effective [13,14]. The EV's energy storage, where today's most common choice is a lithium-ion battery, is often pointed out as the weak component in EVs in these respects. However, rapidly falling costs of 14 % per year for EV battery packs have been reported recently promising lithium-ion batteries to become cost-effective in the near future [13,15]. But more challenges remain. In order to allow for more business cases than EV commuting for all-electric vehicles, an increased electric driving range would be desirable. Also, safety has to be assured and a life time of at least 10 years in vehicle context has to be guaranteed [15].

A reliable state estimation of the battery on-board the vehicle can contribute to solutions for all of these issues. State estimations are essential for managing the battery in order to ensure its safety and optimize its

* In this thesis, the general term "electric vehicles (EVs)" encompasses all-electric or battery electric vehicles (BEVs), hybrid electric vehicles (HEV), and plug-in hybrid electric vehicles (PHEV), see definitions on page 4.

performance and reliability [16]. For example, the battery can be utilized more efficiently so that oversizing, which is expensive and adds weight, becomes unnecessary with a reliable state estimation. Moreover, the battery's life time can be extended by adjusting its operating conditions to an up-to-date state-of-health estimation [17].

Lithium-ion battery performance and state-of-health

Lithium-ion batteries are a family of rechargeable batteries that shuttle lithium ions between their electrodes during charge and discharge. Figure 1 illustrates the working principle of a lithium-ion battery with graphite and lithium nickel manganese cobalt oxide electrodes. During discharge, lithium ions (Li^+) are extracted from the negative electrode and transported via the electrolyte to the positive electrode where they are intercalated. The electrochemical reactions at the electrodes during discharge are:

$$LiC_6 \rightarrow C_6 + Li^+ + e^- \quad (1)$$

$$Ni_{1/3}Mn_{1/3}Co_{1/3}O_2 + Li^+ + e^- \rightarrow Li\ Ni_{1/3}Mn_{1/3}Co_{1/3}O_2. \quad (2)$$

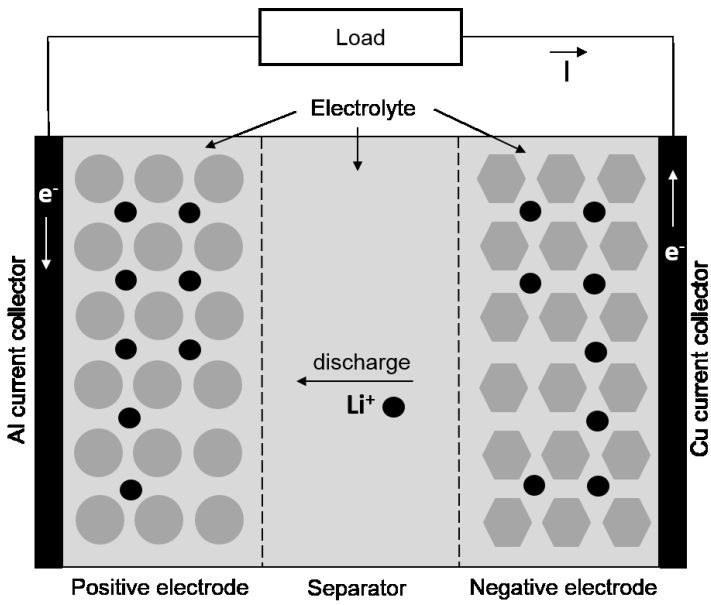

Figure 1 Schematic of a lithium-ion battery during discharge.

The electrons (e^-) released at the negative electrode travel via the current collector through the external circuit where a load such as e.g. an electric motor in an EV can be connected in order to use the electrical energy (current I in Figure 1). The driving force of the current flow is the potential difference between the electrodes. Depending on the choice of electrode materials, a lithium-ion battery provides a cell potential of around 3 to 4 V. A common positive electrode material for automotive lithium-ion batteries is lithium nickel manganese cobalt oxide (NMC) and as negative electrode material graphite and other carbon-based materials are prevalent [18,19]. Apart from the active electrode materials, the electrodes contain a binder and sometimes conductive additives.

The performance of a lithium-ion battery is determined by the processes that occur inside the battery during operation. Performance losses depend therefore on the kinetics of the electrochemical reactions at the electrodes, the mass transport through the electrolyte and in the electrodes, and the contact between the different electronically conducting phases in the electrode. These processes cause voltage losses in a battery cell when a current is flowing. The voltage losses associated with the kinetics (activation losses) are a function of the applied current, just as the contribution from the contact resistance and the part of the mass transport loss that comes from the insufficient ionic and electronic conductivity (ohmic drop) [20,21]. The other part of the mass transport loss is called diffusion resistance (or polarization) as it is coupled to the concentration gradients that build up in the electrolyte and in the electrodes when a current is applied. The diffusion resistance and the voltage drop related to it is thus not only dependent on the applied current, but also on the time that the current has been flowing [21].

Batteries are complex systems whose internal state variables are not accessible with sensors. Therefore, standard performance tests [22,23] to access figures-of-merit of battery performance are established in laboratory testing. Capacity and internal resistance are the two battery properties that capture the most important characteristics of battery performance. Capacity is a measure for the total electric charge that a battery can deliver. Internal resistance is a figure-of-merit for the opposition to a current flow in a battery. “Internal resistance” will be referred to as “resistance” in the remaining thesis summary. Capacity and resistance can be derived from low, constant current discharge tests and

high-current pulse tests respectively. Both capacity and resistance are strongly dependent on ambient operating and load conditions.

Battery performance degrades with time and usage, which is manifested in a decrease in capacity and an increase in resistance. In order to assess the declining battery health, one usually compares the battery's current state variables to their beginning-of-life (BOL) values. According to this, the BOL performance is usually defined as 100 % state-of-health (SOH), a percentage that decreases for degrading battery performance. A battery is often regarded to have reached its end-of-life for vehicle application when one of the battery's performance values has gone below 80 % SOH [24]. Second use of traction batteries in applications with lower performance requirements is therefore a promising market [25,26].

The electrochemically measured loss of battery performance is a result from so-called aging processes occurring in lithium-ion batteries with time and usage. Aging mechanisms have been revealed in different parts of lithium-ion batteries and vary for different battery chemistries. Major reasons for performance degradation are e.g. the formation of resistive surface films at the electrolyte/electrode interface, loss of active electrode material and active lithium, and contact losses in the electrodes [24,27,28]. These aging mechanisms, leading to a higher resistance and a lower capacity have been found to depend on the battery's operating conditions. The load cycle has for example a major impact on the aging of a battery as well as the state-of-charge (SOC) level of the battery [17,29,30]. High temperatures promote not only the rates of the desired electrochemical reactions but also the ones of side reactions [27]. Low temperatures can also have negative effects, e.g. lithium plating during fast charge [31,32].

Lithium-ion batteries in electric vehicles

Most of today's electric vehicles use lithium-ion batteries as energy storage. In all-electric i.e. battery electric vehicle (BEV) systems, the battery pack is the only energy storage whereas in hybrid electric vehicle (HEV) systems, the electrical drive train (battery pack powering an electric motor) is combined with an internal combustion engine with its fuel tank as primary energy storage. The battery in HEV systems can only be charged through the electric motor (used as generator) with energy from regenerative braking or from the combustion engine. In plug-in hybrid electric vehicles

(PHEV), however, the battery pack is designed to be able to receive charge from the electrical grid.

During the application on-board vehicles, batteries are subject to different operation modes such as battery discharge, battery regenerative charge, battery grid charge, and rest. The battery's duty cycle i.e. the demanded charge and discharge current are determined by the driving events and the driver behavior together with the restrictions set by the battery management system. Moreover, the battery is exposed to external operating conditions like ambient temperature, humidity, and vibration.

The operating conditions have a large impact on automotive battery performance. Looking at the example of ambient temperature, lithium-ion batteries perform e.g. badly at low temperatures due to an increasing resistance. As a result, the driving range will drop dramatically [33]. On the other hand, low temperatures are advantageous to store i.e. "park" a battery as self-discharge as well as aging will be slowed down. At temperatures above the comfort range on the other hand, a battery can be discharged much more efficiently, but aging and self-discharge are faster and can seriously shorten the battery's life time [27].

As a consequence from the different architectures of BEV, HEV, and PHEV systems, the requirements on lithium-ion batteries as energy storage in such systems are varying [34]. In BEVs, batteries are operated in so-called charge depleting mode whereas HEV operation is charge sustaining. Under PHEV operation both modes are applied, i.e. charge depleting at higher SOC and charge sustaining at minimum SOC resulting in conflicting requirements for PHEV batteries. A selection of important requirements for automotive batteries is summarized in Table 1. The requirements on the battery's capacity and power specifications result from the operating and system conditions. In order to comply with the power and energy requirements of electric vehicles, lithium-ion battery cells are connected in series and parallel to form modules and packs. Automotive lithium-ion battery cells are preferably adjusted to their specific application in terms of the chosen materials and the system design. For example, an energy-optimized battery cell for application in BEVs will have thicker electrodes than a power-optimized battery cell for a HEV application.

Some battery requirements are however universal for all types of electric vehicles: safety, low cost, long life time, low self-discharge rate, wide operating temperature range, vibration and abuse tolerance – it is a long

list. For most electric vehicle batteries, a low weight and a small volume are also desirable.

Table 1 Requirements on automotive battery systems for application in BEV, HEV, and PHEV. The typical currents are given as C-rate, i.e. the current rate normalized against capacity.

Battery application	BEV	HEV	PHEV
Capacity	High	Low	High
Power	Low	High	High
Typical current	1 C	>10C	3 C

In order to be able to optimize battery systems for the application in automotive traction systems, their on-board usage has to be studied. Laboratory tests under controlled conditions can provide fundamental insight into calendar and cycle life of batteries revealing dependencies on temperature, cycling depth, and SOC [24,27,35]. However, those tests have limited validity for real-life applications as the conditions during vehicle operation are complex as presented above [36–41]. Field tests of traction batteries are therefore an inevitable complement.

As a consequence from the battery's sensitivity to its operating conditions, it is essential to manage it in order to optimize its performance, reliability, and life time. Battery management systems (BMSs) are therefore applied [42,43]. The BMS's primary task is to ensure safe battery operation. This can be achieved by providing accurate measurements of voltage (cell voltages), current, and temperature in order to comply with usage limits i.e. protect the battery from damage like overheating, overcharging, and overdischarging. The SOC estimation is another central task, which is commonly accomplished based on either a combination of Coulomb counting and open circuit voltage (OCV) measurements or equivalent circuit battery models with Kalman filters [44–47]. Ideally, the battery management also makes sure that the battery is used as efficiently as possible by keeping it within its optimal conditions e.g. with the help of cell balancing and a climate system. In order to optimize battery usage, information about the battery's status is necessary. The state estimation can be used in order to assess how much power and energy for vehicle propulsion and other subsystems is available.

This thesis focusses on the state estimation "health". In electric vehicle applications, the battery's SOH is primarily linked to resistance and capacity [14,48,49]. In HEVs, resistance increase is usually the limiting factor, in contrast to capacity fade in BEVs. A reliable SOH estimation enables efficient utilization of the battery, which will lead to lowered costs as the battery does not have to be oversized. Optimizing the battery usage for the battery's SOH will finally result in an extended battery life time. For SOH estimation of batteries, a number of different methods have been suggested in the literature ranging from extensive experimental aging studies via electrochemical physics-based battery models to the previously mentioned equivalent circuit models [29,30,50–55].

Scope and aim of the thesis

The ongoing demonstration of electric vehicles provides a situation where battery operating data from vehicle application is available. In field tests, battery data is collected but it is not necessarily obvious how the data can be used in order to improve for future battery operation. At the same time, conventional battery testing in controlled laboratory environments is still performed. The objective of this project was therefore to make use of the available field data trying to condensate information on the battery from the raw signals and in this way rendering the data meaningful information.

With this starting point, the idea was to make a contribution to the research field mirroring the electrochemical point of view. From this perspective, the battery's instantaneous performance and life time are central. Figures-of-merit that measure battery performance were evaluated and it became apparent that in order to reach the initial goal of evaluating battery usage on-board electric vehicles, a data-driven method to access battery performance measures from the raw data is needed. Consequently, it was decided to develop a method for on-board SOH estimation. The idea was though to keep a close connection to electrochemical methods such as standard performance tests from laboratory testing.

Accessing the battery SOH on-board is, however, not a trivial question as conventional standard tests established in laboratory testing for determination of degrading battery properties such as capacity and resistance are not accessible during constant battery operation. A way to avoid this problem is the usage of a battery model that captures the essential battery behavior. State-of-the-art battery SOH estimation

methods, however, suffer often from a number of shortcomings with respect to on-board application such as battery-specificity, high computational effort, extensive preceding laboratory work or need for operation interruptions or additional equipment [20,29,30,56–60]. Preferably, the SOH estimation method to be developed within this thesis work was therefore meant to accomplish battery performance estimation without these restrictions. Instead it should be inexpensive and easy to implement in the battery management system.

Methods

Within the scope of this thesis, a number of different experimental and modeling methods were applied. To start with, field and laboratory test methods were used to collect battery usage data, followed by modeling methods to derive data-driven battery models that in turn provided access to SOH indicator estimations. As a large part of the thesis work has been method development, the choices and applications of methods for the purpose of information retrieval from battery operating data are research results in themselves.

Battery data collection

The collection of data from battery operation on-board an electric vehicle has to fulfill certain requirements in order to ensure a reasonable data quality enabling a meaningful analysis [61]. As a start, detailed specifications about the battery should be available. The data that is actually monitored during battery operation most importantly has to encompass the battery behavior itself, i.e. voltage, current, temperature, and state-of-charge. Time stamps for those signals are crucial. In order to be able to capture transients, a logging frequency of at least 1 Hz is necessary at least during driving (battery discharge and battery regenerative charge); the frequency can be lower during grid charging and rest times (parking). Current and voltage has to be measured simultaneously and the accuracy of the collected data values has to be sufficient. In addition, the operating conditions in the vehicle (ambient temperature, vehicle speed, vibration etc.) can be interesting. A long-term data collection is a further prerequisite if battery life time is to be studied.

This thesis is based on three sets of battery usage data. One data set originates from the application of a battery pack in the drive train of a PHEV (Paper I). Another data set was produced in the laboratory with a BEV battery cell exposed to a real BEV driving cycle (Paper II-IV). Finally, data from a battery cell mounted on a heavy-duty truck experiencing an emulated HEV environment was used (Paper V).

PHEV battery field test

ETC Battery and FuelCells Sweden AB tested a Volvo V70 plug-in hybrid electric vehicle prototype within the scope of a joint Volvo Cars-Vattenfall project during 2010. The car has been equipped with a 32 Ah Li-ion battery pack whose specifications are summarized in Table 2. Both the behavior of the battery pack and information on the operating conditions were collected with a 2 Hz frequency whenever the ignition was started or the charging cable was connected to the grid [62]. Monitored signals on battery pack behavior were battery pack voltage, battery pack current, battery pack temperature (average of cell temperatures), and battery pack SOC estimated by the BMS provided by the manufacturer with a resolution of 0.4 %). Examples of operating condition signals were date, time, vehicle speed, ambient temperature, and PHEV mode (battery discharge, battery regenerative charge, battery grid charge, diesel drive).

The raw CAN-bus data (controller area network) received from ETC was prepared for further analysis by amongst others extracting only data from battery discharge and battery regenerative charge modes. One driving event for each month of 2010 was selected as exemplified with the current profile during the selected driving event in January 2010 in Figure 2.

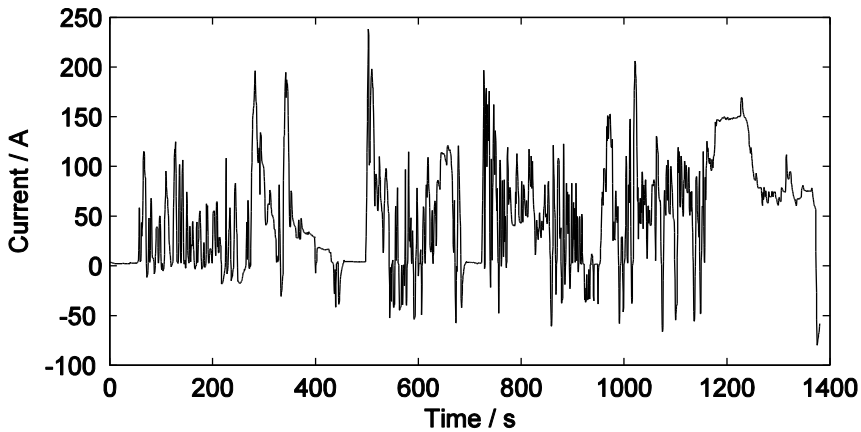

Figure 2 Battery pack current during a selected driving event in a Volvo V70 PHEV prototype recorded by ETC Battery and FuelCells Sweden AB in January 2010. Discharge current is defined positive here as well as in the remaining thesis summary.

BEV battery laboratory test

An automotive lithium-ion battery cell with a nominal capacity of 17.5 Ah (see Table 2 for further specifications) was exposed to a typical BEV current profile in a climate chamber. The current profile was taken from real-life BEV operation (recorded in a C30 Electric by Volvo Car Corporation and scaled down from pack to cell level) constituting an example of a typical commuting driving cycle with a SOC difference of about 15 %. This BEV current profile as depicted in Figure 3 was applied to the cell at four SOC levels (90, 70, 50, 30 %) and five temperature levels (0, 10, 20, 30, 40 °C) that span realistic BEV operating conditions generating the battery usage data for further analysis.

Table 2 Specifications for the three batteries that the data sets in this thesis originate from. Abbreviations used in the table: NMC=lithium nickel manganese cobalt oxide, LMO=lithium manganese oxide, LCO=lithium cobalt oxide, LTO=lithium titanium oxide.

Type	PHEV Li-ion	BEV Li-ion	HEV Li-ion
Number of cells	192	1	1
Weight / kg	150	0.43	0.14
Positive electrode	NMC	Mixed oxide	LMO-LCO
Negative electrode	Hard carbon	Hard carbon	LTO
Maximum voltage / V	395	4.1	2.8
Minimum voltage / V	270	2.5	1.8
Nominal capacity / Ah	32	17.5	3.1
Maximum continuous charge/discharge current / A	250/250	35/35	80/120

Before each current profile test at the respective temperature, standard performance tests were performed: two successive low constant-current (C/3) discharge tests for capacity determination and four 2C (35 A) pulse tests at 90, 70, 50, and 30 % SOC for resistance determination [63]. At 20 °C, some supplementary standard performance tests were conducted: 50 A pulse tests and a synthetic driving cycle test with a maximum current of

35 A as adapted from the ISO standard [22]. An example current profile for each standard test is shown in Figure 4.

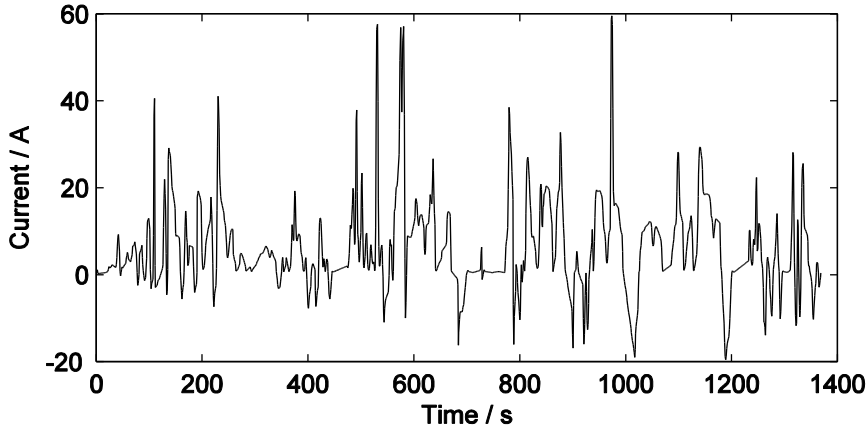

Figure 3 Cell current (downscaled from pack level) during a selected driving event in a Volvo C30 Electric recorded by Volvo Car Corporation in March 2013.

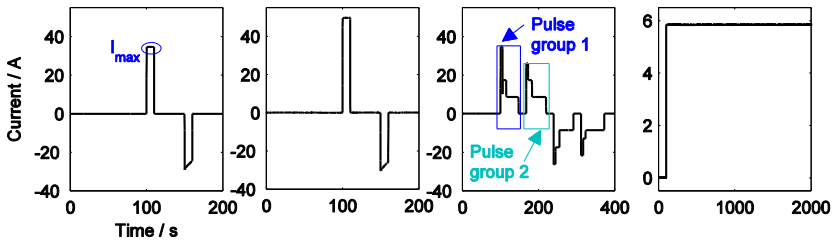

Figure 4 Measured current during standard performance tests of a BEV battery cell at 20 °C. From left to right: 35 A resistance test at 90 % SOC, 50 A resistance test at 90 % SOC, cycle test at 90 % SOC, capacity test.

During these experiments, voltage and current with their respective time stamp were logged with 10 Hz frequency. Temperature and its time stamp were monitored with 1 Hz frequency. From the current I and the time t, the state-of-charge SOC was calculated with conventional Coulomb counting, starting from the fully charged state SOC_{start}=100%:

$$SOC = SOC_{start} - 100 \cdot \frac{\int Idt}{Q}. \quad (3)$$

The capacity value Q was taken from the standard capacity tests at each of the tested temperature levels.

HEV battery field test

Scania mounted a commercial power-optimized cell rated to 3.1 Ah (see Table 2 for further specifications) onto a conventional heavy-duty vehicle where it experienced HEV operation [38]. The HEV environment was emulated by charging and discharging the test cell with the starter battery according to the real-time driving pattern of the heavy-duty vehicle. The field test data used in this thesis was collected between September 2011 and August 2012 and encompassed cell voltage and current recorded with 10 Hz frequency and temperature with 0.1 Hz frequency [64]. The BMS also provided a SOC estimate from Coulomb counting and OCV measurements. An example of a current profile monitored in August 2012 is depicted in Figure 5. About once a month, standard pulse and capacity tests were performed.

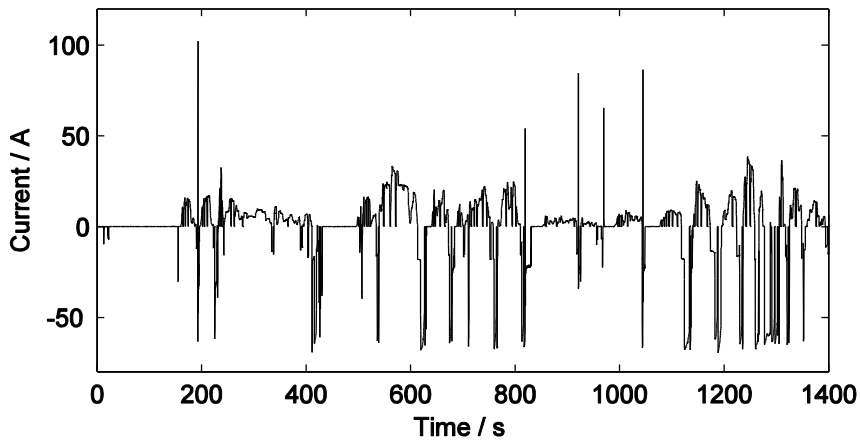

Figure 5 Current of a test cell experiencing HEV operation on-board a conventional heavy-duty truck recorded by Scania in August 2012.

Battery data analysis

The battery data sets were explored in terms of statistics of the single signals, relationships between the signals, frequency content of the signals etc. All activities were conducted in order to learn more about the battery systems that the signals originate from as well as to map how the batteries are used in the PHEV, BEV, and HEV applications. The attained knowledge was applied for designing suitable battery models.

Data-driven battery models

Battery models were created on the basis of the previously presented data sets. In the different papers, models were built with two different modeling techniques (support vector machines or system identification), based on varying model architectures (choice of input and output variables), for different points in time (Paper I and V), and diverse operation conditions such as SOC and temperature levels (Paper II).

Support vector machine-based battery model

Data-driven battery models were created with the help of support vector machines (SVM) in Paper I-III and V [65]. Support vector machine regression is an established machine learning method which has been previously applied to different kinds of optimization problems such as bioinformatics, financial time series, electric load forecasting, and SOC estimation [66–77]. The general idea of this statistical learning method is to find a small number of support vectors out of a large number of examples that still describe a system [78]. A hyperplane approximating the system behavior is optimized from the input/output data. In this thesis, the system "battery" was modeled with the output variable battery voltage from a number of input variables such as current, SOC, temperature, and current history as illustrated schematically in Figure 6. In Paper I, the models are based on the two basic inputs current and SOC for the isothermal case, whereas the models in the proceeding papers incorporate even temperature (Paper II, III, V), and current history (Paper III and V).

Figure 6 Schematic overview of the structure of the created SVM models.

Samples of battery usage data taken from the previously mentioned PHEV, BEV, and HEV data sets functioned as training data, i.e. "learning examples" for the SVM models. In order to minimize the training time, a training data sample which matched the data range of the intended test was selected, as a SVM is only expected to predict well within the trained data range. The selected training data was prepared for SVM training with

the chosen software (SVM^{light} [79]) by scaling the variables X to a [0,1] interval with

$$X_{scale} = \frac{X - X_{min}}{X_{max} - X_{min}} \quad . \tag{4}$$

The upper and lower variable limits X_{max} and X_{min} are listed in Table 3.

Table 3 Upper and lower limits for scaling of the variables included in the battery models based on the three data sets (PHEV, BEV, HEV).

	PHEV data		BEV data		HEV data	
Variable X	X_{max}	X_{min}	X_{max}	X_{min}	X_{max}	X_{min}
Voltage / V	395	270	4.1	2.5	2.8	1.8
Current / A	250	-250	100	-100	120	-120
SOC / %	100	0	100	0	100	0
Temperature / °C	-	-	60	-10	50	-20
Current history variable / A	-	-	100	-100	120	-120

The scaled input/output vectors together with a set of SVM parameters determined from a grid search optimization with cross-validation (Paper I) were read into the program. The training resulted in a SVM model, i.e. a file where the support vectors are listed. The SVM training can be evaluated in terms of training runtime in CPU-seconds (central processing unit) and number of support vectors of the obtained model.

Virtual tests

The derived battery model was used to predict the voltage response of the battery for an input of current, SOC, temperature, and current history. In principle, any other sample of the battery usage data apart from the training data can be used in order to test the performance of the battery models (see e.g. model validation in Paper I and V). As the goal of this thesis is the development of a method for on-board SOH estimation, the battery models were used as an information source of battery properties. The black-box battery models were thus chosen to estimate the voltage response for virtual tests corresponding to standard performance tests established in laboratory testing for determination of resistance and capacity. For the cases that standard performance test validation data was

available (Paper II- V), the monitored real current and temperature as well as the calculated SOC and current history variables served directly as input data for the virtual tests. The input variables were scaled prior to SVM test, just as for the SVM training. The voltage estimation $X_{estimated}$, which the SVM software returned for a certain virtual test and SVM model, was compared to the voltage measured in the real standard tests $X_{measured}$, which represented the experimental validation. The voltage estimation performance was evaluated in respect of the (maximum and average) relative error *RE* of the voltage estimation in %,

$$RE = 100\ \% \cdot \frac{|X_{estimated} - X_{measured}|}{X_{measured}} \quad , \tag{5}$$

and the root-mean square percentage error *RMSPE* of the voltage estimation in %,

$$RMSPE = \sqrt{\frac{1}{n}\sum_1^n RE^2} \quad , \tag{6}$$

where *n* is the number of estimations. In Paper I, where no validation was available, a hypothetical standard test was applied just as it would be like in the intended application of the method on-board a vehicle.

Inclusion of current history

In Paper III and V, the battery model has been complemented with a current history input variable as indicated above. In addition to current, SOC, and temperature, different current history variables were evaluated in terms of their ability to improve the time-dependent estimation performance of the battery model. The investigated current history variables were derived by applying different weight functions of time to the current vector for a specified period back in time. The different weight functions of time are shown in Figure 7. The simplest evaluated function was the unweighted mean of the current for 100 s back in time. The other moving current averages were weighted with the reciprocal square root of time for two different time windows and an exponential weighing factor with different time constants [21,80–82]. Just as the other battery model input variables, the current history variables were scaled prior to SVM training (see Table 3).

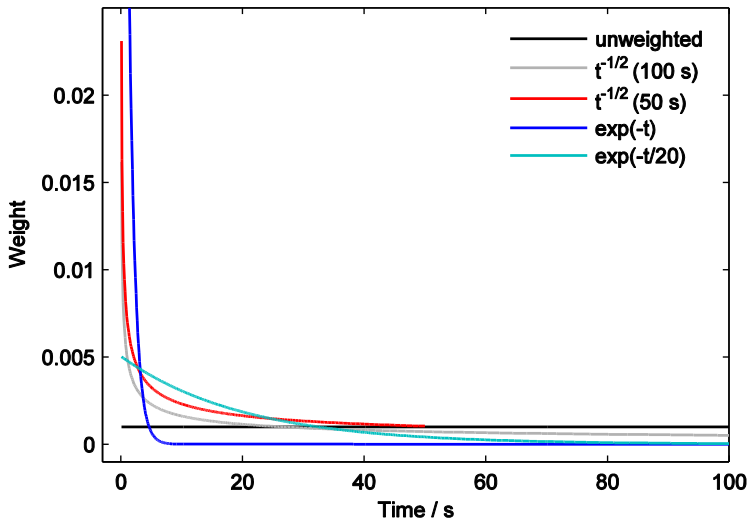

Figure 7 Weight functions of time used to treat the current vector in order to derive different moving current averages as model input variable. The first values of the exp(-t) function, which are close to 0.1, have been truncated in favor of the visibility of the other functions.

System identification battery model

In Paper IV, dynamic battery models were obtained with a system identification approach [83,84]. System identification means the derivation of mathematical models of dynamic systems from measured input-output data with statistical data-driven methods. The model structure, which was suggested based on an analysis of the BEV battery laboratory data, was a current input and a voltage output with SOC and temperature being part of the model parameters. The used model structure, which is derived with an equivalent circuit battery model as starting point with an autoregressive exogenous model (ARX), was

$$v(k) = (a+1)v(k-1) - av(k-2) + b_0 i(k) + b_1 i(k-1) \qquad (7)$$

where $v(k)$ and $i(k)$ are the dynamic voltage and the current and the index k is the uniform discrete-time instant. a, b_0, b_1 are the model parameters to identify. When the model parameters are known, the resistance for a certain constant current pulse can be calculated analytically.

Capacity and resistance estimation

Capacity and resistance values were determined from real and virtual standard performance tests. In Figure 8 and Figure 9, examples of voltage responses during such standard tests are given. For the respective current profiles of the shown pulse and capacity tests it is referred to Figure 4.

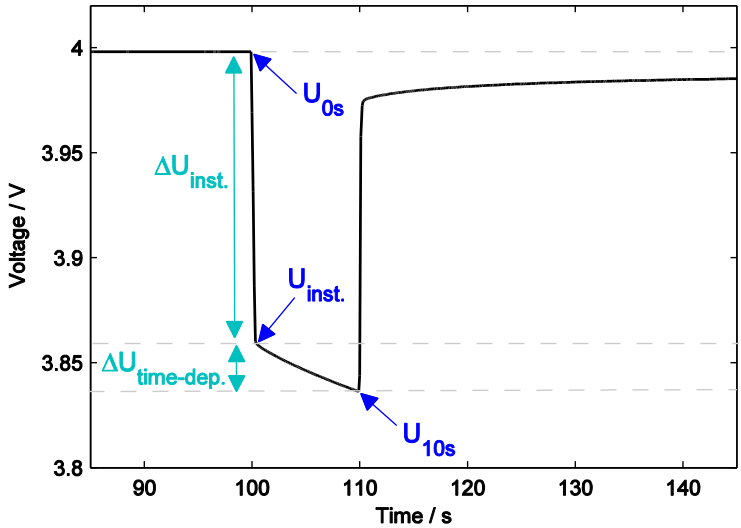

Figure 8 Measured voltage of a BEV battery cell during a standard resistance test at 20 °C (2C-discharge pulse at 90 % SOC).

The internal resistance of a battery may be determined from pulse tests. A battery at open circuit is exposed to high-current charge and discharge pulses resulting in voltage rises/drops caused by the battery's resistance. Resistance determination is exemplified in Figure 8 for the 10 s discharge resistance of a BEV battery cell from the voltage during a 35 A discharge pulse. The 10 s discharge resistance R_{10s} is obtained from the value of the applied current I_{max} (see Figure 4) and the voltage drop U_{0s}-U_{10s} , where U_{0s} is the open circuit voltage at a specified SOC and temperature, and U_{10s} is the voltage under discharge after 10 s (as indicated in Figure 8):

$$R_{10s} = \frac{(U_{0s}-U_{10s})}{I_{max}}. \quad (8)$$

The voltage drop during the I_{max}-pulse can be divided into an instantaneous voltage drop,

$$\Delta U_{inst.} = U_{0s} - U_{inst.}\,, \tag{9}$$

and a time-dependent voltage drop,

$$\Delta U_{time-dep.} = U_{inst.} - U_{10s}\,, \tag{10}$$

where $U_{inst.}$ is the voltage directly after the current is applied. The instantaneous voltage drop, i.e. the initial steep drop, is related to the activation losses, contact resistances, and ohmic drop in the battery, whereas the further drop during the pulse comes from diffusion resistance and the SOC decrease.

Different resistances were looked at for the batteries studied in this thesis depending on the specifications of the battery under test, the intended application of the battery, and for the case of the virtual tests even the availability of training data. The 10 s discharge resistance over a 35 A (2C) pulse with its contributions was used as SOH indicator for the BEV battery cell in Papers II-IV. In Paper III, additional resistances from 50 A discharge pulses and pulse groups in the performed cycle tests were derived (see indications in Figure 4). The PHEV battery pack in Paper I was evaluated with a 10 s discharge resistance over a 65 A (0.26 C) discharge pulse and for the HEV battery cell (Paper V) 18 s discharge and charge pulses with a current rate of about 20 C (60 A) were used for resistance determination.

Capacity is the charge that a battery can deliver between specified voltage limits. Discharge capacity is thus determined from a low-current discharge from the maximum to minimum specified voltage. Figure 9 illustrates the concept for the example of a BEV battery cell being fully discharged at C/3 rate from the upper voltage limit of 4.1 V to the lower limit of 2.5 V. The discharge capacity Q is calculated by numerically integrating the current I (see Figure 4) between these voltage limits over the discharge time t:

$$Q = \int I dt. \tag{11}$$

The capacity test in this form has been applied in Papers II-IV. The virtual capacity tests have been restricted to partial discharges from 4.1 V to 3.875 V and 3.0 V respectively (as indicated in Figure 9) according to the range of the available training data. For the same reason, the 2.5-2.4 V capacity was estimated for the HEV battery cell in Paper V although the

real standard test was a constant current discharge at approximately 2 C from 2.8 to 1.8 V.

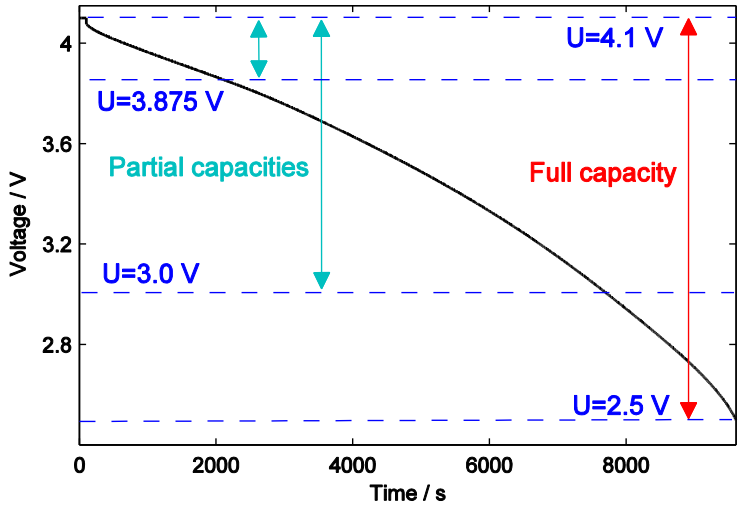

Figure 9 Measured voltage of a BEV battery cell during a standard capacity test at 20 °C (full constant current discharge with C/3-rate).

The determination of resistance and capacity from estimated voltage responses, i.e. the so-called virtual standard tests, gave access to estimations of resistance and capacity for a battery under operation without actually performing a real standard test. The accuracy of these resistance and capacity estimations based on the virtual tests was evaluated when an experimental validation (real test) was available. For that purpose, the relative error (RE, Equation 5) of the estimations of resistance, resistance contributions, and/or partial capacity was consulted. If many estimations were performed, e.g. for varying operating conditions (SOC, temperature, time), the root-mean square percentage error (RMSPE, Equation 6) or average RE were given.

Capacity and resistance are essential battery properties that degrade with time and usage, which makes them important SOH indicators. In the thesis studies based on the BEV data, it has been looked at snapshots of these SOH indicators at one moment in time. For the PHEV and HEV data (Paper I and V), however, the development of resistance/capacity of the respective battery was actually followed over time.

Results and discussion

The results and discussion chapter summarizes the main results of this thesis spanning the whole spectrum from battery data collection and statistics to the developed SOH estimation method and its vehicle application scenario. The core results are the support vector machine-based battery models whose voltage estimation performance during virtual driving and standard tests is presented as well as their SOH indicator estimation capability and briefly their computational performance. Results from the alternative battery modeling method system identification are also shortly stated.

Analysis of battery data collection

This section starts out with an example of collected battery data in order to give insight into issues that were found to be important for battery data collection. An extract of the results from the laboratory testing of the BEV battery cell are shown in Figure 10. The shown recordings at 20 ^{o}C for current, voltage, and temperature encompass a sequence of two capacity tests, four 35 A pulse tests at different SOC, and finally four BEV current profile tests at the same SOC levels.

As this example is taken from laboratory measurements, the accuracy of the measured signals current, voltage, and temperature is good. Under on-board conditions the quality of the monitored signals is generally not as good as a consequence of less accurate measuring equipment and less control over the operating conditions. This can be observed e.g. for the voltage measurement in the HEV field study where small jumps of the size of ~ 0.01 V occur as can be seen in Figure 18.

In the experimental procedure in Figure 10, rest periods are integrated in order to allow the BEV cell to relax before each test. For example, after the one-hour rests subsequent to a full discharge, the OCV still increases marginally as Figure 10b reveals. Such slow dynamics are typical for energy-optimized batteries as commercial BEV cells. This behavior is in contrast to commercial power-optimized HEV cells as used in the HEV study where the OCV can already after a few tens of seconds of rest be used for OCV measurements for SOC estimation purposes (see Paper V).

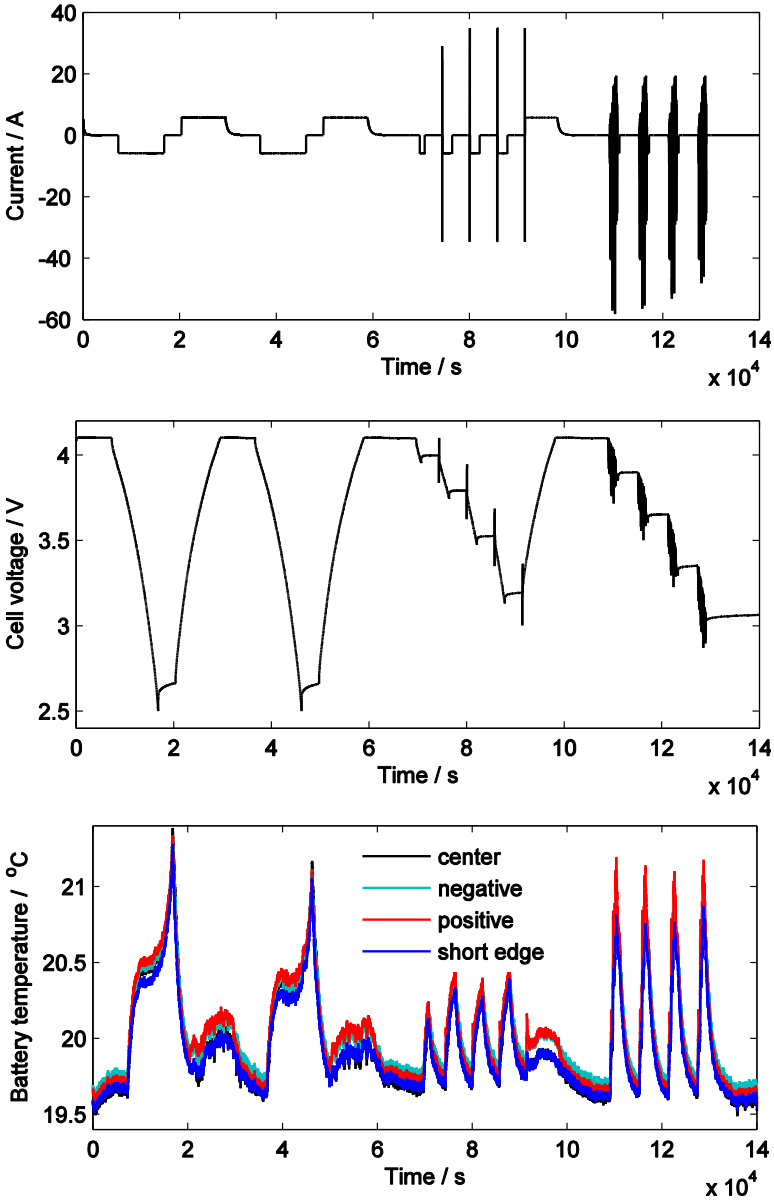

Figure 10 Example of data collection results from the tested BEV battery cell. Measured (a) current, (b) voltage, and (c) temperature during standard performance and current profile tests of the BEV battery cell at 20 °C.

Battery temperature measurements are an intricate topic. Ordinarily, only temperature measurements from sensors on the battery cell surface are available. As can be observed in Figure 10c for different positions on the tested BEV battery cell's surface, already the surface of a single battery cell can show temperature gradients although the temperature increases during the applied current profile are very moderate (~2 °C). The temperature inside a battery cell is often unknown as temperature sensors inside a cell are problematic. One tries therefore to access estimations of the inner battery temperature via models [85]. Thermal battery models can also be consulted in order to understand time shifts which can be observed between processes happening in the cell and the manifestation in a measured surface temperature decrease or increase (see Figure 10c in relation to Figure 10a and b).

When instead of a single cell a battery pack composed of hundreds of cells is to be monitored, the amount of data to possibly collect is huge. Commonly it is focused on a reasonable amount of data, e.g. temperature sensors only on module level, but still single cell voltages for safety reasons. The temperature distribution issues mentioned above are obviously more severe for full battery packs than single cells [86], necessitating battery management strategies for cell balancing and climate control.

Battery data statistics

The characteristics of battery behavior under PHEV, BEV, and HEV operation were investigated with the help of statistics. To exemplify, a comparison between typical PHEV, BEV, and HEV operation is discussed.

From the battery's perspective, the operation time at a current is important. Figure 11 compares therefore the operating time at different C-rates for typical PHEV, BEV, and HEV current profiles from Figure 2, Figure 3, and Figure 5. The current from these profiles is given on cell level normalized against cell capacity (see Table 2 for specified capacities). The BEV and HEV battery currents are already on cell level whereas the PHEV battery pack current and capacity need to be divided by two (96S-2P configured battery pack i.e. two strings of 96 cells in series connected in parallel).

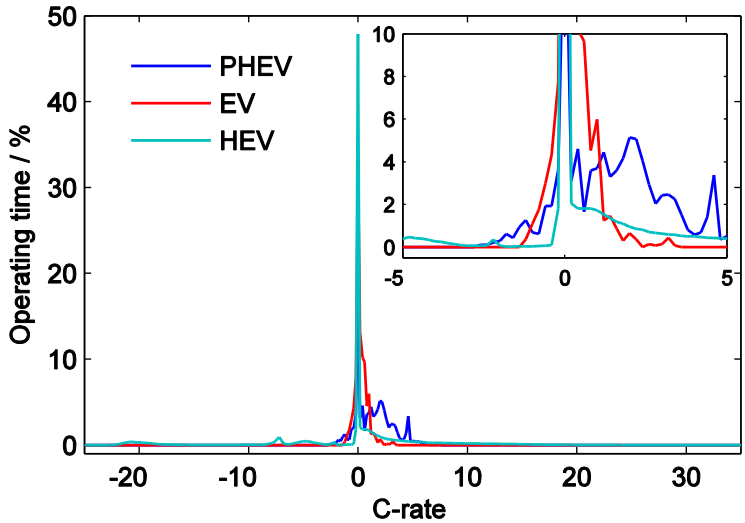

Figure 11 Operating time at C-rate levels (intervals of 0.2 C) for the respective example operating profile from the PHEV, BEV, and HEV test (based on the current profiles from Figure 2, Figure 3, and Figure 5).

The distribution of C-rates in Figure 11 illustrates the significant differences between BEV, HEV, and PHEV battery usage. Naturally, the time share between charge and discharge differs for the three applications with HEV showing a more balanced division than the BEV and PHEV batteries that are mostly discharged during the driving cycles. The BEV battery delivers low discharge rates a major part of the operating time whereas the HEV battery is operated a considerable amount of time both at high charge and discharge rates. As Table 4 clarifies with maximum and mean C-rate values extracted from Figure 11, the PHEV values lie inbetween the BEV and HEV values.

From a comparison between the actually occurring C-rates in these typical operating profiles with the specified maximum continuous charge and discharge current rates (Table 2), it can be concluded that the used batteries are oversized in some respects for their respective application. Especially the charge rates hardly reach up to the specified maximum continuous charge current rates which are lower than the maximum peak rates.

Table 4 Maximum and mean discharge and charge rates for the C-rate distribution for the studied PHEV, BEV and HEV batteries from Figure 11.

Battery type	Discharge rate / C		Charge rate / C	
	Maximum	Mean	Maximum	Mean
PHEV	7.5	1.8	-2.5	-0.7
BEV	3.4	0.5	-1.1	-0.3
HEV	33.2	2.0	-23.1	-9.6

Another important characteristic of a current profile are the current dynamics. The frequency content of the three example current profiles differs a lot. In comparison, the frequency content of the BEV current is dominated by low frequencies. The frequencies of the PHEV and HEV current are higher (see Figure 2, Figure 3, and Figure 5).

Support vector machine-based battery model

On the basis of the collected battery usage data, support vector machine-based battery models were built in Papers I-III and V.

In Paper I, SVM models were derived from PHEV battery field data. Figure 12 visualizes the hyperplane resulting from training a SVM with voltage, current, and SOC data from a 23 min driving event in January 2010 with a battery pack temperature ranging from 20 to 29 ^{o}C. The overall trends are a voltage decrease with decreasing SOC and with increasing discharge currents, which is in accordance with fundamental battery characteristics.

The model structure with SOC and current input and voltage output was expanded in the papers subsequent to Paper I, adding temperature and time dependence by appending temperature and current history variable inputs.

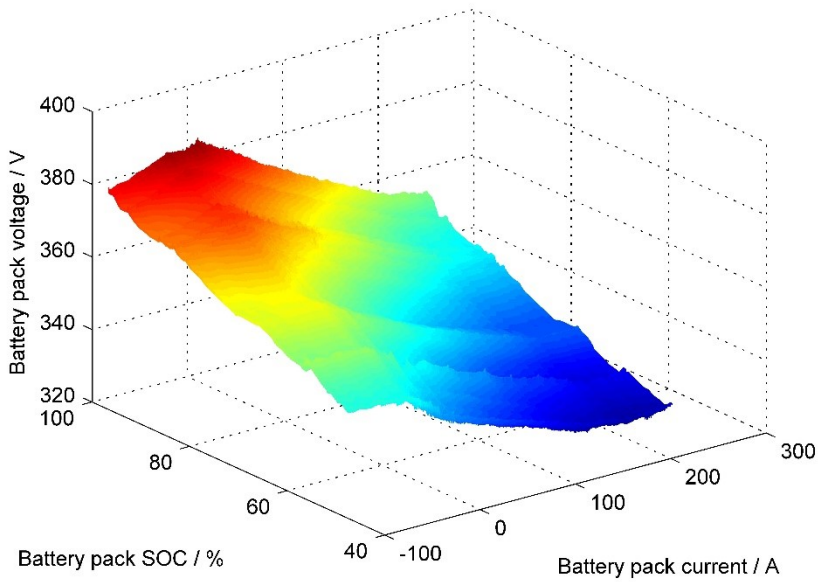

Figure 12 SVM-based battery model based on training data from a PHEV driving event in January 2010 [87].

Battery models of this type were derived with SVM^{light} [79], a SVM implementation in the programming language C. Within the scope of the SVM training, the dimensionality of the system is increased to a space where the system is linear with the help of a kernel trick. A number of other SVM parameters have to be chosen to solve the optimization problem [88]. These SVM parameters were tuned with a grid search approach where the training runtime of SVM^{light}, the number of support vectors (SVs), the maximum relative error as well as the RMSPE served as assessment criteria [89,90]. As a result from this investigation, a radial basis function kernel with kernel option γ=14 was selected. The soft-margin parameter C=1.0134 and the size of the ε-insensitive loss function ε=0.01 were chosen. The parameter tuning was done on the basis of the SVM test and model from Figure 13. In order to show that the suggested SOH indicator estimation method is applicable independently of the studied battery or application, the same set of SVM parameters was applied in Papers I-III and V.

Voltage estimation performance

The derived SVM-based battery models as exemplified in Figure 12 were used to estimate the battery voltage for different test scenarios. Mainly in order to verify the model, the models were tested with data similar to the data it was trained with i.e. current, SOC, and possibly temperature and current history from other driving instances. The second type of test scenario were the so-called virtual standard tests where the SVM battery models are tested in order to gain information on the respective battery's SOH.

Driving data tests

The driving data test in Figure 13 is the one which was used for SVM parameter tuning as mentioned in the previous section. The accurate voltage estimation of the SVM model for this driving data test is reflected in a maximum relative error of 1.4 % and a corresponding RMSPE of 0.28 %. As the estimation was performed with a temperature-independent model it was important to find two driving instances for training and test with similar temperature level. 2-fold cross validation (switching of training and test data) gave slightly higher error values (max. RE=1.5 % and RMSPE=0.40 %) since the new test data exceeded the data range of the new training data.

Figure 14 shows another driving data test for an example from the HEV field test. Here, the error values for the voltage estimation performance of the applied current history model are a maximum RE of 2.7 % and a RMSPE of 0.54 %. These values lie in the same order of magnitude as the previously derived estimation performance for the PHEV field test example. The error values are however slightly higher compared to the PHEV driving data test although a more elaborate model with current history was applied in contrast to the temperature-independent basic model. For better comparability to the PHEV test, the same HEV data driving test was therefore also performed with a basic model instead of a current history model yielding a maximum RE of 5.9 % and a RMSPE of 0.68 % (results not shown). The higher voltage estimation errors of the HEV test example in comparison to the PHEV case can be due to a number of reasons.

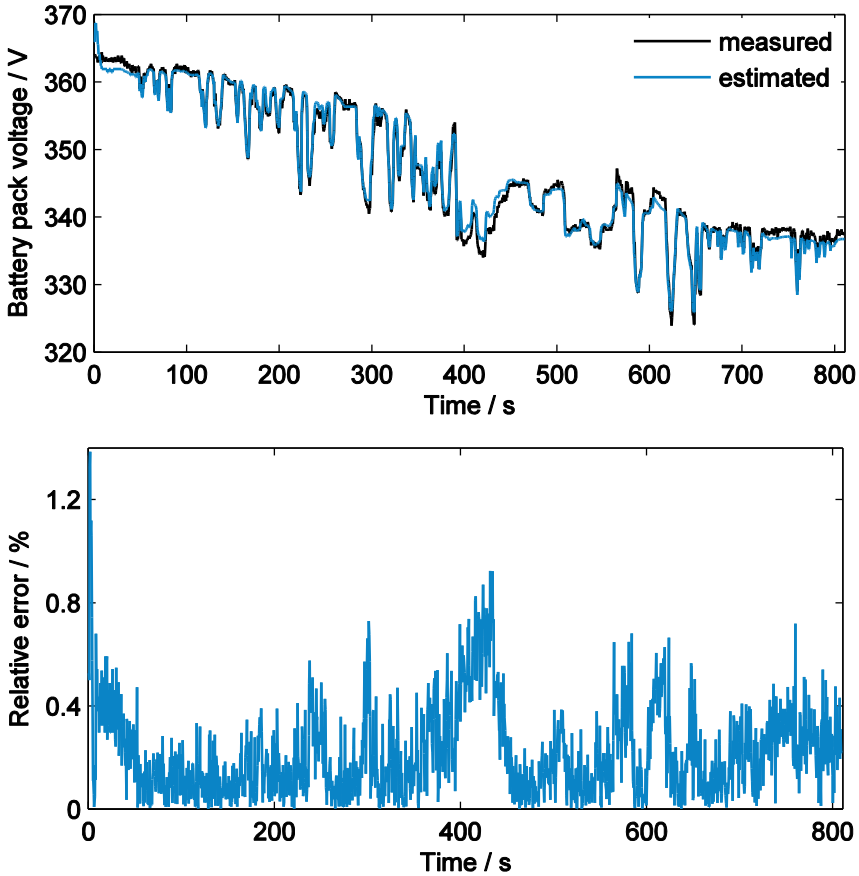

Figure 13 (a) Estimated and measured PHEV battery pack voltage. The estimation is based on a SVM model from 25 min training data in April 2010. A 14 min PHEV driving event from March 2010 served as test data. (b) Relative error of the voltage estimation.

The SVM parameters are for example not specifically tuned for this HEV driving event. Further on, higher current rates occur in the HEV profile than in the PHEV profile, which poses larger challenges on the non-linear estimation performance of the model. This fact can be investigated by comparing the appearance of high relative errors with the corresponding current in Figure 5. The corresponding SOC and temperature curves are also more eventful than for the PHEV data.

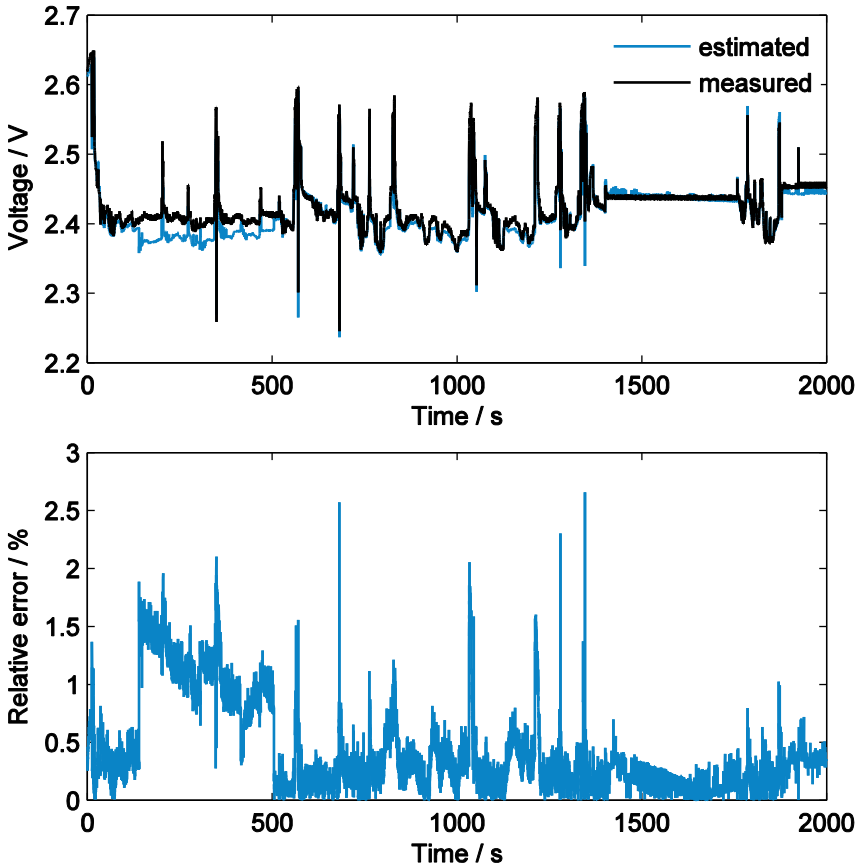

Figure 14 (a) Estimated and measured HEV battery cell voltage. The estimation is performed with a SVM-based current history model based on 2.75 h training data from the cycling period 2011-11-07 until 2011-11-30. 33 min driving data from the same cycling period served as test. (b) Relative error of the voltage estimation.

Virtual standard tests

After verifying battery models with driving data, it was proceeded to hypothetical test scenarios that correspond to standard performance tests in order to access capacity and resistance estimates.

Figure 15 and Figure 17 give examples of such standard test scenarios as applied for the BEV battery cell. The validation i.e. the real standard tests for three types of pulse tests (Figure 15) and one capacity test (Figure 17) are overlaid with the corresponding virtual tests on basis of a number of

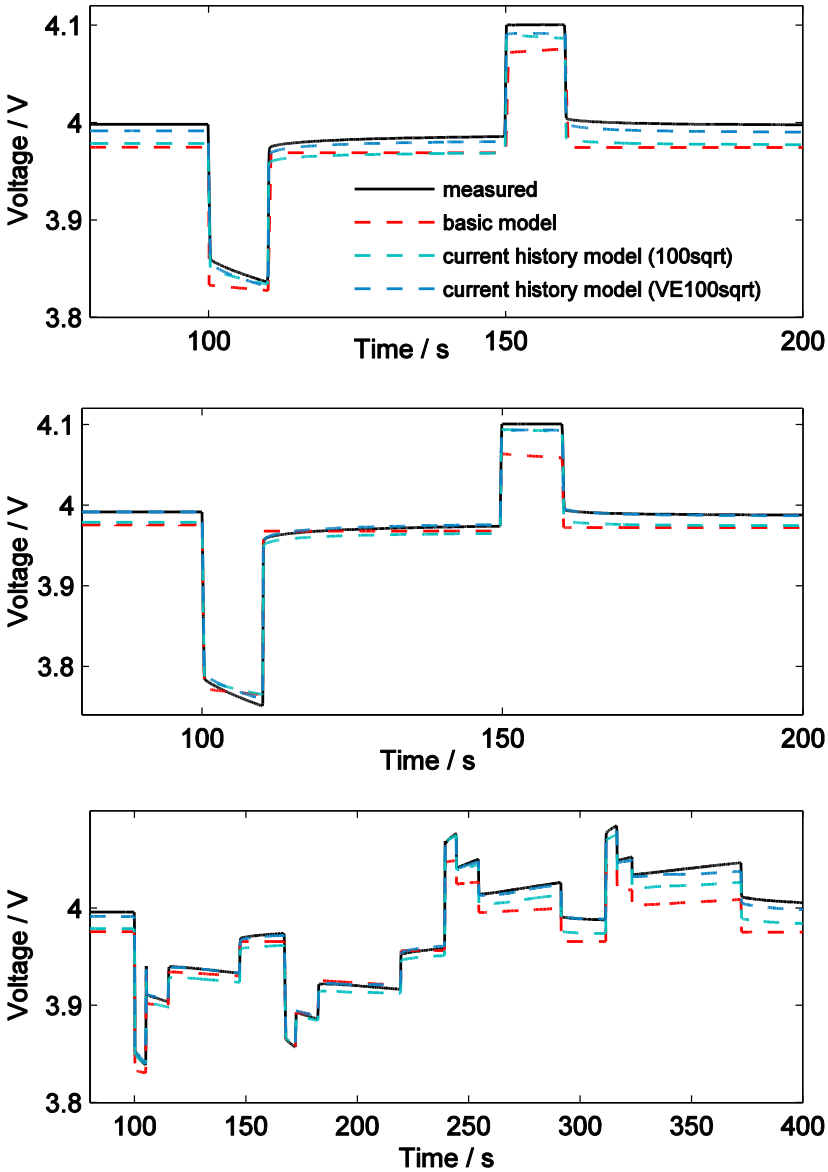

Figure 15 Measured and estimated voltage responses of a BEV battery cell during different standard tests (90 % SOC, 20 °C). (a) 35 A resistance test, (b) 50 A resistance test, (c) cycle test. The voltage estimations are from the basic model and the current history models “100sqrt” and “VE100sqrt”, see p. 31 for definitions.

different SVM-based battery models. The shown battery models are the basic model i.e. the model that relies on a current-SOC-temperature input for voltage estimation (in red), as well as two current history models that have an additional current history input variable. One of the current history models, which is named “100sqrt” (in green), integrates the current history input directly into the basic model whereas the other model “VE100sqrt” (in blue) applies a two-step voltage estimation where in a first step a basic model is used for voltage estimation followed by a second step that estimates the voltage estimation error (VE) of the first model with a “100sqrt” current history model. The denotation “100sqrt” indicates that the additional current history variable is a current moving average weighted with a reciprocal square root of time-weighing factor applied for a time window of 100 seconds. This weighing factor was shown to perform well out of a selection of several weighing functions that were investigated in Paper III.

Both the basic and the current history models reproduce the general pattern of the measured voltage response of the battery to the sequences of current pulses and rests (Figure 15). The inaccuracy of the voltage estimations during the relatively high current charge pulses of 35 A and 50 A demanded in the resistance tests can be explained by those current rates lying outside the data range of the BEV driving training data. Therefore, the following analysis will disregard this part of the test profile.

A closer look at Figure 15 reveals the differences in estimation performance of the different displayed models. The basic model can neither capture the OCV levels before the current pulses accurately nor the dynamics of the battery voltage during pulses and the subsequent relaxation periods despite satisfactory voltage estimation performance figures with RMSPE around 0.5 % (Figure 16). The “100sqrt” current history model on the other hand can describe the trends during pulse and relaxation accurately although the initial voltage level is not correctly localized. Those improvements result in better RMSPE as Figure 16 shows. The current history model “VE100sqrt” eventually fulfills an accurate voltage estimation during all these situations, both during the initial OCV period, the current pulses, and the subsequent rest periods. These observations from Figure 15 apply to a varied extent for the three different studied current profiles. The voltage estimation of the “VE100sqrt” model during the 50 A resistance test is partwise almost indistinguishable from the measured voltage response with a RMSPE of 0.07 %. For the other tests,

the 35 A resistance test and the cycle test, the estimations are slightly inferior but still very accurate (see RMSPE in Figure 16). In summary, the estimations of this current history model are a large improvement from the basic model estimations.

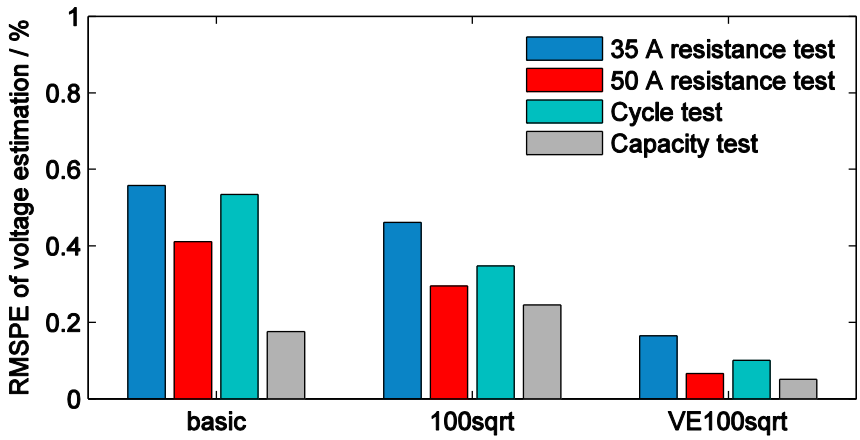

Figure 16 RMSPE of the voltage estimation of three SVM models during four virtual standard tests (see color code in the figure). See p. 31 for definitions of the basic model and the current history models "100sqrt" and "VE100sqrt".

The processes in the battery resulting in the voltage response (see introduction on p.3) can clarify the different models' estimation performance. The dynamic voltage behavior is connected to the diffusion processes in the battery, which gain importance during long and high current pulses. Through the addition of a current history variable to the model input, this time dependence can be accounted for. The basic, static model, however, cannot capture those dynamic effects and thus the estimated voltage drop during the discharge current pulses is only a result from the linked SOC decrease.

The estimation performance of the different models in the case of the virtual capacity test is displayed in Figure 17. As Figure 16 reveals, the basic model delivers already an accurate estimation with 0.2 % RMSPE. This value can be improved to 0.05 % by the "VE100sqrt" model although diffusion processes should not play a major role in low constant current situations. As already observed for the case of the resistance tests, the "VE100sqrt" current history model, however, substantially improves the estimation of the initial voltage value.

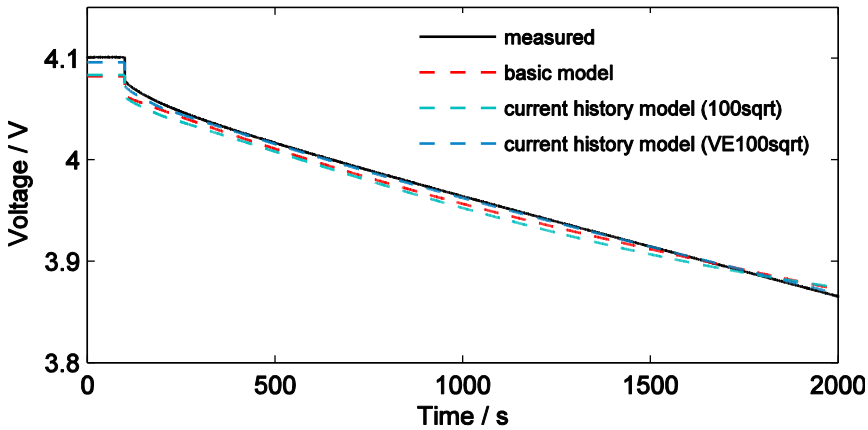

Figure 17 Measured and estimated voltage responses during a capacity test of a BEV battery cell at 20 °C. The voltage estimations are from the basic model and the current history models "100sqrt" and "VE100sqrt".

Moving from virtual standard tests for the BEV battery cell to another example, Figure 18 and Figure 19 show an example of estimation and validation results for standard pulse and capacity tests in the scope of the HEV field study.

With respect to the potential computational restrictions of the intended on-board application of the suggested SOH indicator estimation method, the two-step voltage estimation models ("VE"-models) were disregarded in this study. The direct current history models (e.g. the "100sqrt"-model) provide, however, an accurate voltage estimation even during the extremely high current pulses of 20 C in the pulse test profile as Figure 18 verifies. This is in contrast to the basic model, which also in this example reaches its limitations. The voltage estimation of the "100sqrt"-model is however precise in all situations from the location of the initial SOC level, via the instantaneous voltage drops when a current is applied, to the dynamic behavior during the high and low current pulses. For a discussion of the sloping voltage behavior during the relaxation periods, which is related to the current history's time window of 100 s, please consult Paper V.

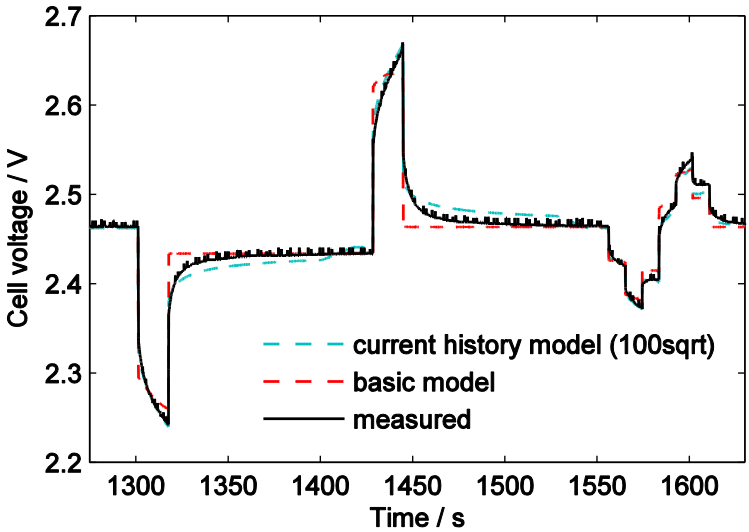

Figure 18 Measured and estimated (with basic and current history model) voltage responses of the HEV battery cell during the standard pulse test on 2011-11-29. The high current (20 C) and low current pulses at 50 % SOC are shown.

In Figure 19 displaying the corresponding capacity test overlain with the voltage estimations from the current history and the basic model, it is obvious that the models estimate poorly outside the trained SOC. The two models estimate the voltage however accurately within the trained data range. This fact raises the question if there are meaningful figures-of-merit that can be defined for typical HEV operation, which is characterized by a narrow SOC operating window. For capacity determination, it is natural to change the cut-off voltages of the current integration and account for a partial capacity instead. This partial capacity will encompass the battery's actual application, and if aging effects occur within the narrow SOC range they will be noticed. However, it is questionable to which extent such a partial capacity figure-of-merit can be used as an overall SOH indicator. Degradation that occurs in the beginning and end of the discharge curves cannot be followed, only capacity fade that is visible in the part of the discharge curve that is covered by training data can be detected. For the middle part of the discharge curve aging could be manifested by a general voltage drop or a change in the slope of the curve with time and usage [64,91,92].

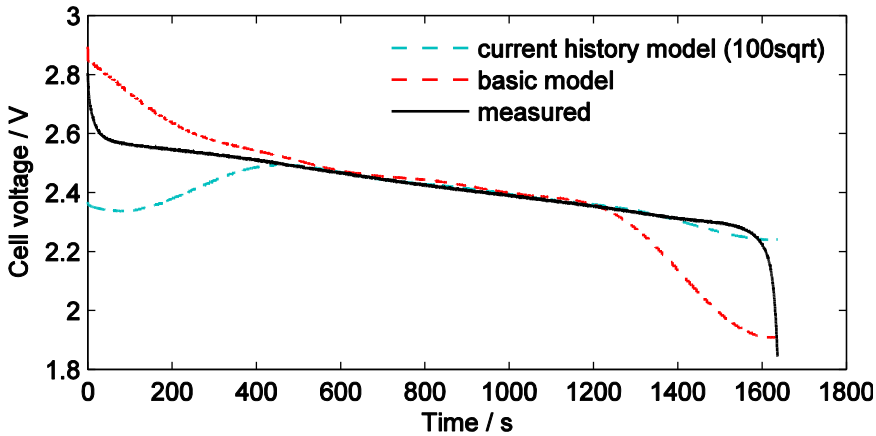

Figure 19 Measured and estimated (with basic and current history model) voltage responses of the HEV battery cell during the standard capacity test on 2011-11-29.

A general issue with the virtual test approach is that the usage situations that the models are trained on are quite unlike the standard test situations. Very roughly it can be stated from a comparison of the presented standard tests in comparison to typical PHEV, BEV, and HEV operation as e.g. in Figure 11 that a standard capacity test with a constant low discharge current is rather representative in terms of current magnitude whereas constant currents are unusual in ordinary vehicle application. Standard pulse tests on the other hand are often composed of pulses of unrealistically long pulse length and high current magnitude. Anyway, the estimation quality derived with the battery models shows that meaningful results can be achieved. This circumstance gives, however, reason to reconsider the design of standard test situations that are far from the real usage. Today's standard battery performance tests are certainly valid for 'extreme' situations, but ideally, standard tests should account for typical driving as well as for extremes. A possible approach to tackle the different characteristics of driving and standard test cycles is thus the suggestion of new standard tests that are closer to the real operation. For that purpose, simple synthetic tests representative for real-life application from driving statistics could be created with the help of e.g. Markov chains [93].

Capacity and resistance estimation

On the basis of the presented virtual and real test results, capacity and resistance data have been determined. In this section, results from the BEV battery data set, where a broad coverage of different operating conditions was available, are presented and discussed.

The results from the 35 A resistance tests at five temperature levels for the BEV battery cell can be found in Figure 20. As elaborated in the section on capacity and resistance estimation in the methods chapter, the figure-of-merit resistance as derived from a standard pulse test can be divided into two contributions. Both the instantaneous and the time-dependent voltage drop are shown in Figure 20.

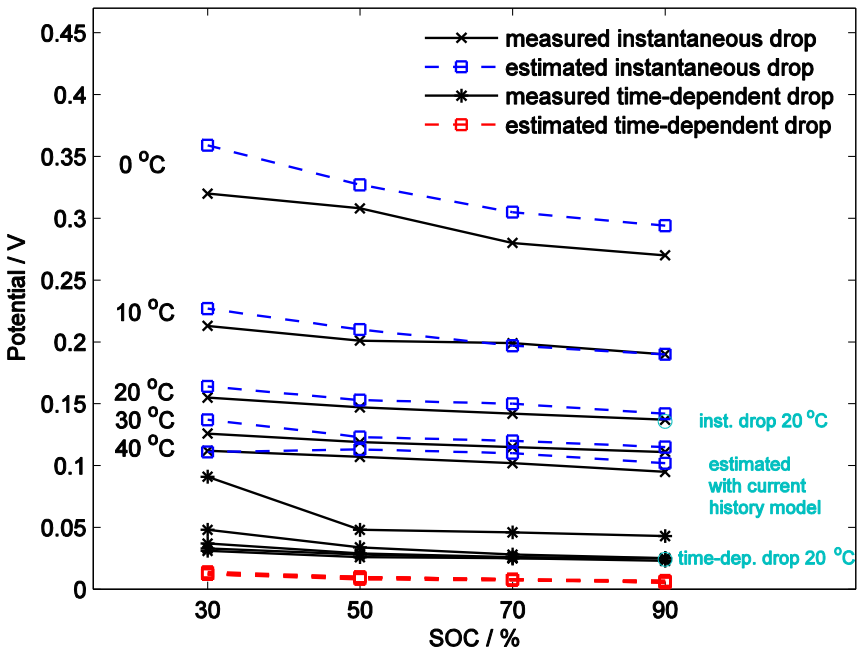

Figure 20 Instantaneous and time dependent voltage drop of a BEV battery cell for the temperature interval 0-40 °C at different SOC. Both measured and estimated (with the basic model: blue and red, with the current history model "VE100sqrt": green) values are given for a 35 A discharge pulse over 10 s.

Looking at the validation results separately first, the instantaneous voltage drop contribution (x) to the total resistance is only slightly influenced by different SOC levels for one temperature for this BEV battery cell. The

effect of temperature on the instantaneous voltage drop is more pronounced. Figure 21 points also out the temperature dependence for the case of the total resistance at 90 % SOC. Those observations are in accordance with experimental studies on battery cells with comparable chemistry [30]. The time-dependent drop contribution (*) that is shown separately in Figure 20 accounts only for around 17 % of the total voltage drop for this cell and current pulse. It does not show a large SOC or temperature dependence. At 0 °C however the time-dependent voltage drop is significantly larger than at the other temperature levels and low SOC increases this trend.

The estimations of the instantaneous voltage drop with the basic SVM-based battery model (blue, □) are accurate for all studied temperatures apart from the 0 °C level, where the estimation significantly overestimates the voltage drop. At the other temperature levels, the estimations also show a slight overestimation in most cases whereas the best estimations are achieved at moderate temperatures and high to medium SOC. For the operating condition, where a current history model was evaluated, the estimation result is indicated in green (○). The current history model's estimations are very precise both for the instantaneous voltage drop and particularly for the time-dependent voltage drop. As already mentioned in the previous section on virtual standard tests, the basic model cannot capture the time-dependent, diffusion-related voltage behavior during a long current pulse apart from the connected SOC decrease during a discharge pulse. Therefore, all time-dependent drop estimations of the basic model for the different temperatures end up at the same result (red, □).

Figure 21 combines the two resistance contributions to a total 10 s discharge resistance for the case of the 90 % SOC level. There is an obvious gap between the measured resistances and the resistance values estimated with the basic model. This "gap" i.e. the diffusion resistance can be overcome by including current history in the battery model as the result at 20 °C shows. The basic model delivers a resistance estimation of 4.26 mΩ for the measured 4.66 mΩ whereas the current history model reaches as close as 4.61 mΩ, i.e. a relative error of 1.1 %.

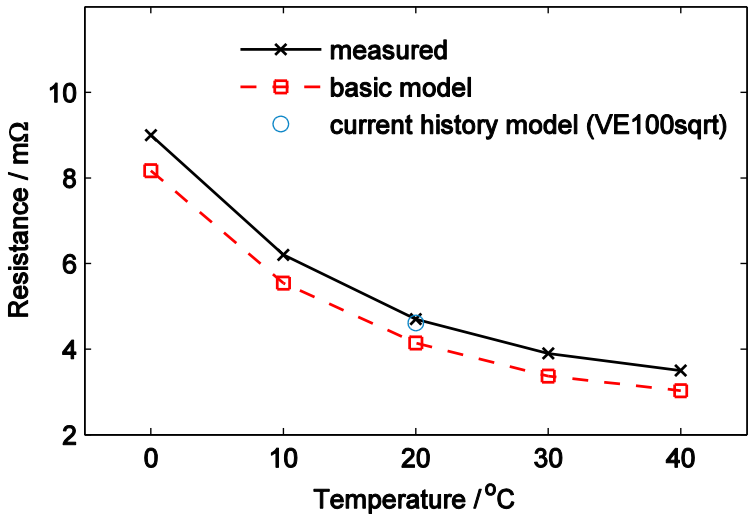

Figure 21 10 s discharge resistance of a BEV battery cell at different temperatures as derived from a 35 A discharge pulse at 90 % SOC. Both experimentally derived values and estimations from two battery models are given.

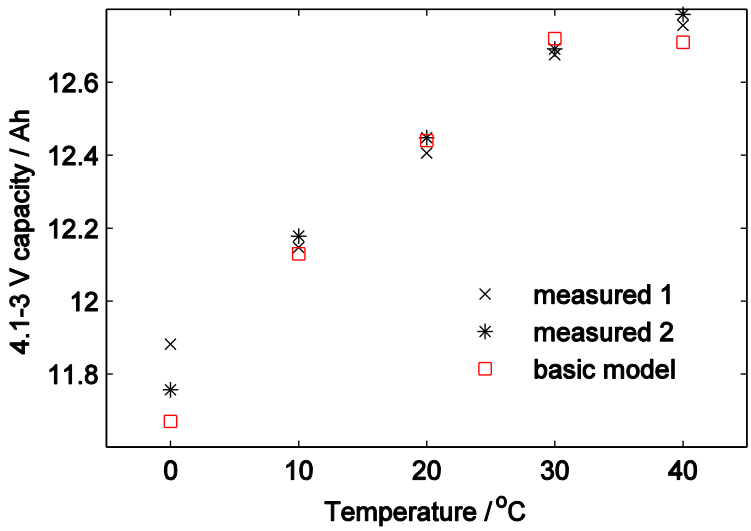

Figure 22 4.1-3.0 V capacity of a BEV battery cell at different temperatures. Both the results from two measurements and the estimation with the basic model are given.

The experimental capacity test results for the BEV battery cell for two consecutive full discharge tests are shown in Figure 22. The capacity increases for increasing temperature as expected. The RMSPE of the basic model estimations is 0.63 %, i.e. an estimation very close to the laboratory results although even the measured results deviate significantly for the two measurements at least for the 0 ^{o}C temperature level.

In the capacity figure, only the 4.1-3.0 V partial capacity estimated by the basic model (Paper II) is shown as the current history model was used to only estimate the 4.1-3.875 V capacity at 20 ^{o}C (Paper III). The derived 4.1-3.875 V capacity values were a measured value of 2.93 Ah, a basic model estimation of 3.02 Ah, and a "VE100sqrt"-model estimation of 2.96 Ah. The current history model actually achieves an even more improved capacity estimation (1 % RE) from the already good basic model estimation (3 % RE).

Computational performance

The suggested SOH estimation method poses a number of computational requirements. Firstly, a certain memory is needed in order to store driving data for SVM training. Then, the SVM training itself requires processing power, followed by the SVM tests. The SVM test results, i.e. the SOH indicators and probably even the SVM models i.e. the support vectors, have to be stored online in order to be available for future reference.

The SVM training runtime is very dependent on the structure of the model and the number of examples in the training data. In an example from Paper I, a SVM training based on 1775 examples took 1.6 CPU-s and resulted in 339 support vectors. The computational performance results from Paper II reveal that for more expansive data sets of up to around 880,000 examples, long training runtimes are needed (in the order of 10^5 CPU-s). The number of SV on the other hand stays reasonably small even for these expansive data sets (~10,000 SVs). Generally, the SVM training time requirements grow not only with the number of examples, but also with the number of model variables. In Paper III it was however found that the inclusion of an additional model input (current history) can return faster training runtimes and reduced number of SVs for the resulting models. It was thus found to be meaningful to include current history even from the model complexity respect.

A way to minimize training runtime is to make a selection from the training data. The data selection should be based on matching the driving data to the intended virtual tests. This concept was verified in Paper II where it was shown that the estimation performance of resistance at a certain SOC was similar for models spanning the whole and only partial SOC ranges. The SOC level-limited models were however preferable in the respect of accumulated training runtime.

The SOH estimation itself, i.e. the SVM tests are very fast for the test sequences applied in this thesis. The virtual tests are therefore found to be unrestrictedly suitable for online application.

System identification battery model

An alternative battery modeling approach has been evaluated. With the help of a system identification approach, dynamic battery models according to Equation 7 were built for data sets from the experimental study on the BEV battery cell (Paper IV). The model structure was based on a single input-output relationship between current and voltage with model parameters depending on the SOC and temperature conditions. This model structure was derived starting from an equivalent circuit model approximation, which was formulated as an ARX model, whose order has been adjusted. During the model derivation, the direct connection with the physical circuit elements was therefore lost indicating that the actual dynamic relations in the battery are more complex than the equivalent circuit model. The method estimates the dynamic voltage response for a current input at a SOC and temperature level. The initial OCV is to be incorporated in the model in the scope of future work.

20 different models were created based on the available typical BEV operating current profiles for the studied SOC and temperature condition range. Figure 23 shows an example of a model estimating the dynamic voltage response for a 35 A pulse test. All models provide an accurate dynamic voltage estimation.

The resistance estimations based on the derived models are good as well as Figure 24 illustrates for the case of the resistance estimations at 10 ^{o}C at the studied SOC levels. The resistance estimations at 10 ^{o}C can be obtained with an average RE of 2.1 %. These error values compare to the estimation

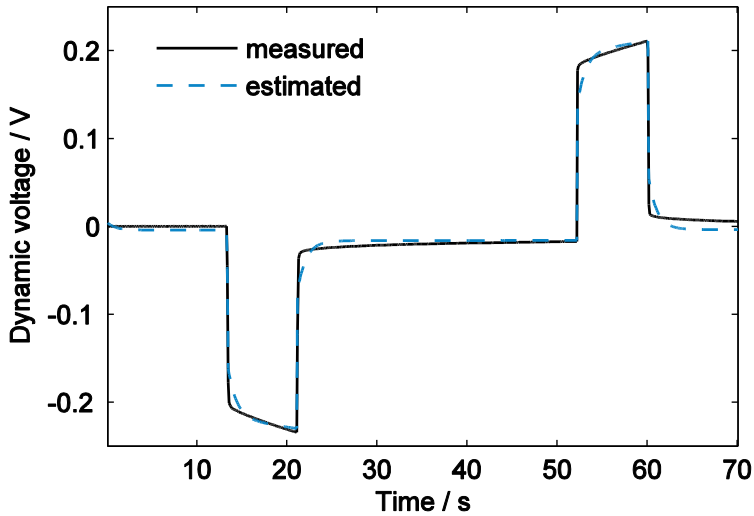

Figure 23 Measured and estimated (with a system identification approach) dynamic voltage (initial OCV not included) of a BEV battery cell during a 35 A pulse test at 50 % SOC and 10 °C.

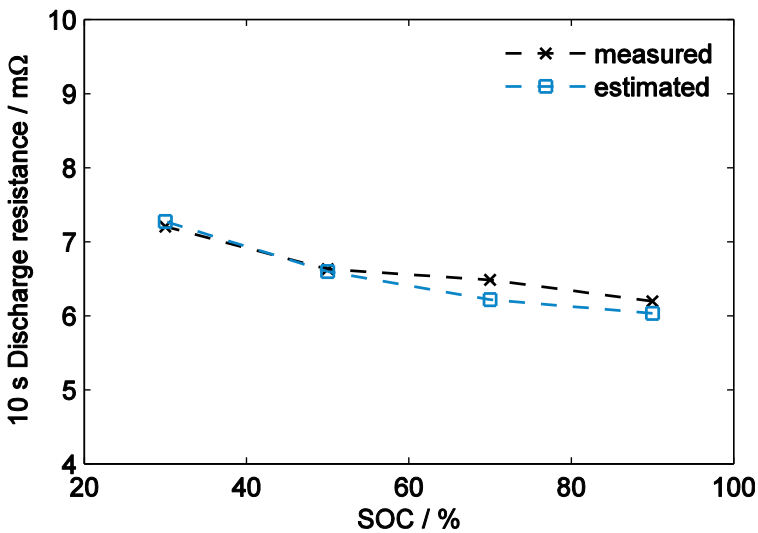

Figure 24 Real and estimated (with a system identification approach) values of 10 s discharge resistance of a BEV battery cell at different SOC as derived from a 35 A discharge pulse at 10 °C.

performance of the basic SVM model for the same resistance values at 10 °C with an average RE of 8.4 % (error values based on results as exemplified in Figure 21). Addition of current history to the basic SVM model, however, gave improved resistance estimation as the example of the resistance estimation at 90 % SOC and 20 °C by the current history model "VE100sqrt" shows which was achieved with a RE of 1.1 % (as mentioned above, Figure 21).

An advantage with the system identification approach in comparison to the support vector machine approach is the possibility of estimating the uncertainty of the estimation result. The uncertainty of the derived resistance estimations can be derived by propagation from the uncertainty of the identified model parameters. Very narrow uncertainty intervals are obtained, about three orders of magnitude smaller than the range of the resistance values. Consequently, the derived models and their resistance estimations can be trusted.

With respect to computational load in terms of on-board applicability, the resistance estimation with this method is very fast as it is only based on a linear identification. The parameters of the model are found by solving a simple linear least squares problem.

Developed state-of-health estimation method

In this final section of the results chapter, the developed SOH estimation method is described in the context of its intended application. Figure 25 illustrates schematically how the method could work in vehicles. As an example, whenever an estimate of the battery's health condition is desired, a sample from collected battery operating data e.g. for 30 min of preceding driving or for certain operating conditions such as current, SOC, or temperature levels is selected. The data sample is then used by the BMS to compute a battery model capturing the current characteristics of the battery system. Any data-driven battery modeling method such as SVM or system identification could be used in principle. In a next step, the battery model could be tested virtually with the desired virtual capacity or resistance test in order to access an up-to-date estimate of these SOH indicators. These estimates can then be used by the BMS in order to manage the battery (see Figure 25) and to update the battery's SOH in relation to previously estimated capacity and resistance values.

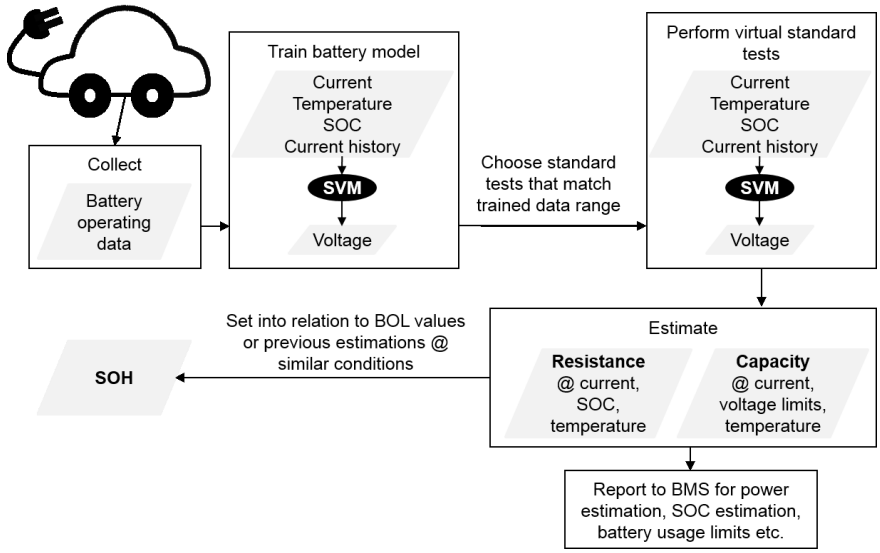

Figure 25 Schematic overview of the developed SOH estimation method in a vehicle implementation scenario. As battery modeling approach, SVM-based battery models are shown.

This approach could theoretically be used for all kinds of batteries in all kinds of applications and is not limited to the studied applications BEV, PHEV, and HEV. In the scope of this thesis, however, the SOH indicators have been followed with this method over one-year periods for the PHEV and the HEV field tests (Paper I, V).

In the PHEV field test, which served as a proof-of-concept in the scope of this thesis, 10 s discharge resistances were estimated. The resistance estimations were based on virtual 65 A (0.26 C) discharge pulse tests at 90 % SOC for PHEV battery data samples from each month of 2010. These estimations were performed with a temperature-independent basic SVM model i.e. the voltage estimation was only based on SOC and current as model input. The resistance estimation results for the chosen driving events over the one-year period are shown in Figure 26. As a result from the shifting temperature levels over the seasons, the obtained resistance estimates range from 98 to 185 mΩ. Figure 27 illustrates therefore the correlation of the derived resistance estimations with the average value of the battery pack temperature during the respective driving event. The

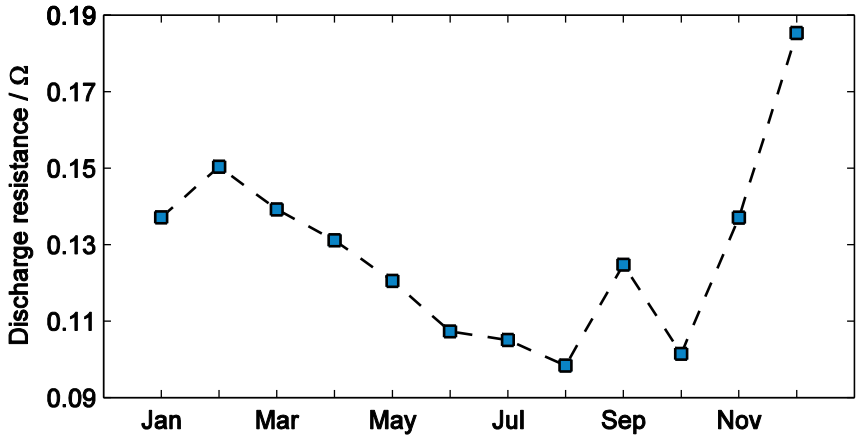

Figure 26 Estimated 10 s discharge resistance of a PHEV battery pack as derived from virtual 65 A pulse tests on temperature-independent basic SVM models based on driving events from January to December 2010.

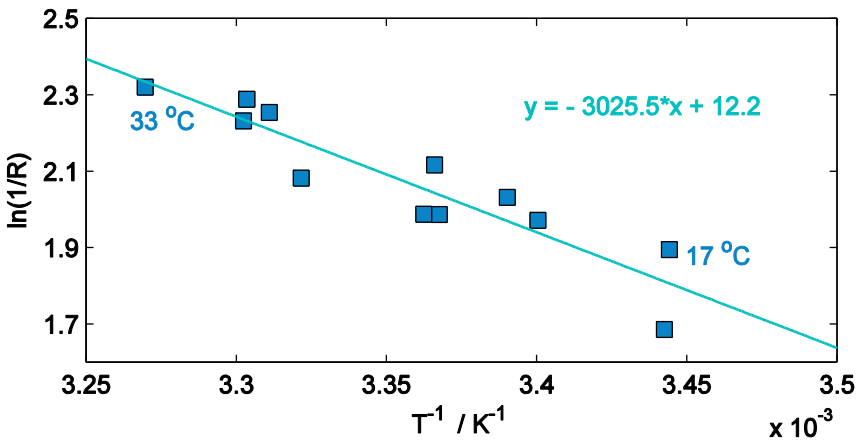

Figure 27 Arrhenius plot of the 10 s discharge resistance of a PHEV battery pack (Figure 26) against average value of the battery pack temperature during the respective driving event. A linear trend line indicates the correlation between the two variables (R^2=0.8524).

correlation between these variables is quite strong (with coefficient of determination for the linear fit R^2=0.8524) indicating that the observed variation in discharge resistance over the one-year period is mainly temperature-related. As temperature explains such a large part of the resistance estimation variations, it can be concluded that no significant

resistance increase due to battery aging has been taken place during the time period of the field study. This example of strong temperature dependence of the resistance illustrates the importance of an accurate temperature measurement for proper differentiation of temperature and degradation influences on the battery's resistance [94].

In contrast to the PHEV field study where the battery pack resistance was reported, the results from the HEV field study are on cell level. In a battery pack, the battery pack resistance is derived from the sum of the single cell resistances that are connected in series and the reciprocal sum of parallel connections. Wiring, contacts etc. have also an impact on the total battery pack resistance. The cell resistances for the PHEV battery pack consisting of 192 cells with a 96S-2P configuration should therefore approximately be in the order of magnitude of 2 to 4 mΩ for the considered temperature range according to,

$$\frac{1}{R_{pack}} = \frac{1}{96 \cdot R_{cell}} + \frac{1}{96 \cdot R_{cell}}, \tag{12}$$

where R_{pack} is the battery pack resistance and R_{cell} the cell resistance.

The resistance of the studied HEV cell happens to lie in the same order of magnitude although totally different conditions apply and the cells have different chemistries and specifications. The 18 s charge and discharge resistance is evaluated for the HEV cell from 20 C charge and discharge pulses at 50 % SOC at 25 °C. The measured and estimated charge and discharge resistances as well as partial capacities are summarized in Figure 28 for the one-year field test period. The measured resistances and capacities do not show pronounced degradation trends during the test period. The observed variations can be explained with small differences in the standard test conditions such as temperature, pulse length, and current rate. Therefore, instead of reporting SOH percentages, only values of capacity and resistance are given.

The resistances are estimated with the current history model "100sqrt" whereas the capacity is derived on the basis of the temperature-dependent basic model. From the accumulation of large capacity estimation errors of up to nearly 50 % from May to July 2012, a software problem could be detected where an erroneous capacity value was reported to the BMS. Apart from this software problem causing particularly high capacity estimation errors, the estimation errors are on a high level also the rest of

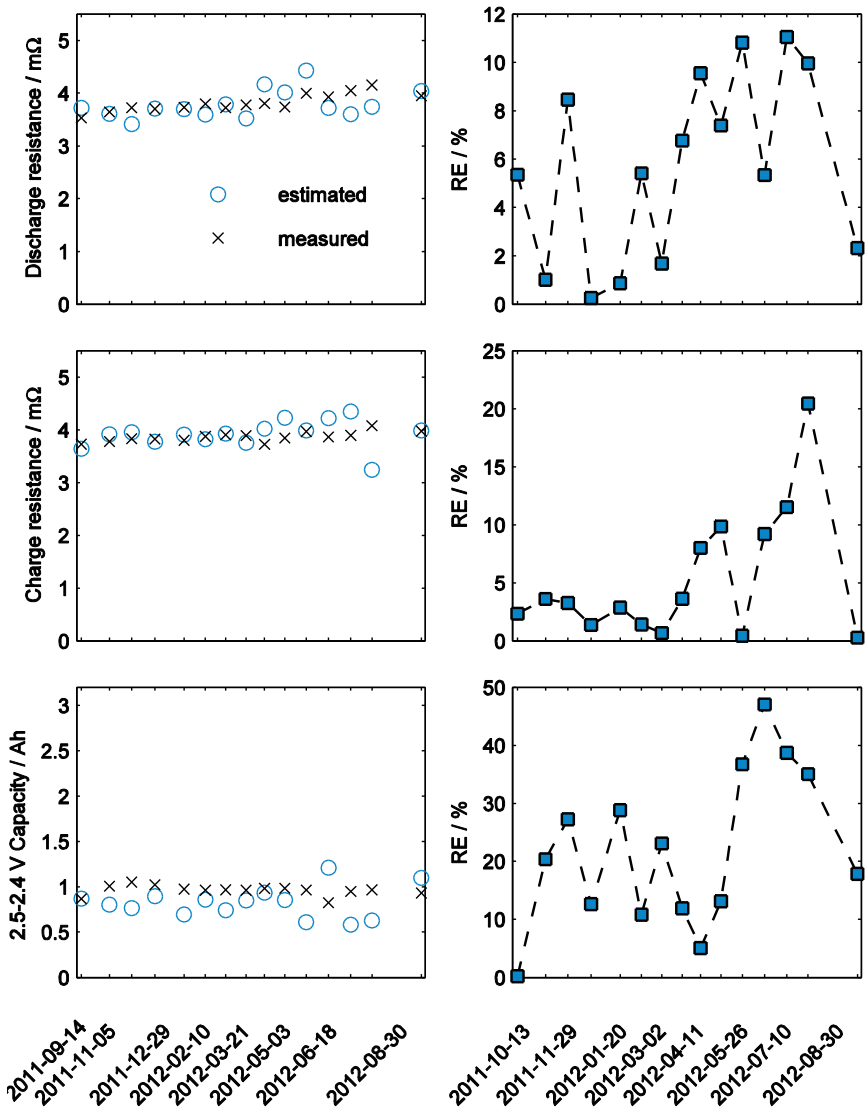

Figure 28 SOH indicator estimation results for the HEV field test at different dates during a 1-year period. Estimated (o) and measured (x) values (on the left) as well as relative error of the respective estimation (on the right) for (from top to bottom) 18 s discharge resistance, 18 s charge resistance, and 2.4-2.5 V capacity.

the year with an average relative error of 16 %. Capacity estimation is a challenging task for data-driven battery models in HEV applications where the SOC operating window limits the available training data. In addition, the studied HEV cell is characterized by a very flat voltage curve making a correct SOC estimation difficult.

The resistance estimations at 50 % SOC on the other hand worked out well as plenty of training data was available. The average error of the discharge resistance estimations in Figure 28 is 5.7 % and the charge resistance estimations can be estimated with an average relative error of 5.3 %. These estimation accuracies can be considered acceptable for on-board SOH indicator estimation.

Although field data has been used in this thesis, the models and virtual tests have been computed offline subsequent to the field test periods on a conventional desktop computer so far. In order to demonstrate the SOH estimation approach for on-board application, the implementation of the SOH estimation method in a research concept vehicle has been conducted in cooperation with Integrated Transport Research Lab [95]. In the scope of this Mechatronics student project, a suitable hardware platform with sensors, appropriate computational capabilities and CAN interface was selected as well as the software for the prototype battery management system was designed [96].

As hardware platform BeagleBone black with an add-on printed circuit board was chosen. As software, a QNX real-time operating system with three daemons for collection, training, and calculation (virtual test) with CAN functionalities was used. The developed platform can sense current, temperature, and voltage, compute SOC, run SVM trainings and virtual resistance and capacity tests, and report SOH through the CAN interface. The definitive implementation in the scope of this project was, however, prevented by a short circuit in the voltage measuring module during the testing of the final prototype.

To summarize, with the help of the suggested SOH indicator estimation method, estimates of inner battery properties that normally stay unknown in black box modeling can be accessed. Resistance and capacity estimates derived via the introduced virtual standard tests provide SOH indicators that conveniently can be compared to test results from established laboratory testing.

Conclusions

A method for battery state-of-health (SOH) estimation on-board electric vehicles has been developed. The approach gives access to battery SOH indicators only based on data readily available from the battery management system (BMS) without any experimental preparation or need for preliminary battery information. This makes the method very versatile. Basically without changes to the model design, the method has therefore been conveniently applied to battery data from BEV, PHEV, and HEV operation i.e. a variety of different batteries, operating conditions, and usage patterns.

In the scope of the thesis, recommendations for battery data collection have been compiled (e.g. the importance of sufficiently high logging frequencies) and issues of battery data collection have been pointed out (e.g. the difficulty of accessing valid temperature measurements). The collected battery data has been analyzed statistically highlighting the characteristics of BEV, HEV, and PHEV battery operation in terms of e.g. current rates, charge and discharge time share, and frequency of current pulses. The usage analysis has shown that all three studied batteries are oversized in respect to their typical operation, aging not considered.

From on-board battery usage data, data-driven battery models were created. As data mining method, the established support vector machines (SVM) were chosen, which have not been previously applied for battery voltage and subsequent SOH estimation as in this project. This SVM method is found to be a powerful tool for handling large amounts of battery operating data at a reasonable computational load.

The applicability of the SVM approach for the SOH estimation task was demonstrated. However, limitations with data-driven modeling techniques have also been identified e.g. the restriction of estimations to the training data range. Another traditional criticism of data-driven models, a high computational load, has however been shown to be manageable with appropriate data preparation and selection. Apart from the SVM-based battery models, another modeling approach, i.e. system identification, has been evaluated and found to be suitable since the method gives accurate resistance estimations and is fast and simple.

The derived SVM-based battery models have successfully been verified on driving data, where they have shown to describe the battery behavior accurately. Within this thesis work, several different model structures were evaluated whereas the most elaborated model architecture was a current/temperature/state-of-charge (SOC)/current history-input in order to predict the voltage output. The current history input is a new feature that is rarely found in data-driven battery models. This time-dependent variable has been shown to be able to account for the effects of diffusion resistance on the battery voltage dynamics.

Applying virtual tests that correspond to standard performance tests to the derived black-box battery models gave access to SOH indicator estimations such as capacity and internal resistance. This is a very convenient tool as virtual tests can be validated with established laboratory tests and the SOH estimations based on the virtual tests correspond to meaningful battery figures-of-merit as derived from real standard tests. The SOH indicators capacity and resistance have been followed over one-year time periods in order to demonstrate their feasibility for the SOH estimation task.

The suggested method can be implemented into the battery management system of an electric vehicle in order to monitor the SOH of the traction battery from the measured signals voltage, current, and temperature, and the BMS's SOC estimation.

Acknowledgements

I would like to thank everybody who contributed to my thesis work in different ways:

To my supervisors Göran Lindbergh and Mårten Behm for giving me the opportunity to work on this exciting research project and for guiding me scientifically.

To the Swedish Hybrid Vehicle Centre for funding my project.

To everybody who was engaged in giving me access to real-life battery data, from engineers to lawyers. Particularly to Viktor Ekermo (ETC) and Carl Göranson (Volvo Cars), and to all the others: Bengt Axelsson, Theresa Granerus, Anders Bern, Patrik Larsson, Elin Löf, and Goran Widborn (Volvo Cars), Pontus Svens (Scania), Christina Engström (KTH Legal department), Filip Kjellgren (Consat), Egil Mollestad (Think).

To Stefan Arnborg (KTH) for introducing me to support vector machines, and to Arne Elofsson (Stockholms Universitet) for discussion SVM usage.

To my collaborators Pontus Svens (Scania), Giuseppe Giordano, and Jonas Sjöberg (Chalmers) for valuable synergies.

To Peter Georén (KTH Transport Labs) and the team of Mechatronics students for pursuing the implementation of my method.

To my present and former colleagues at Applied Electrochemistry (and even at Energy Processes) for enjoyable lunch and fika breaks and also for your nice company during conferences. A special thanks to Ann Cornell for guidance in teaching and to Carina Lagergren for being helpful in all types of contexts. Finally, to my fellow PhD students within the field of batteries (Simon, Maria, Henrik, Pontus, Matilda, Tommy, Jonas, Andreas) for our discussions, giving feedback to each other, informative journal clubs etc.

To my friends Leefke and Heike for our weekly swim workouts and amusing lunch chats.

To my parents and my sister Juli for being so positive about me living in different places in the world and visiting a lot.

To my little family, Johan and Paulina, for being the sweetest imaginable delay of my doctoral studies.

References

1. 2011 – Hamburg. (2015). at <http://ec.europa.eu/environment/europeangreencapital/winning-cities/2011-hamburg/>
2. ARCADIS Sustainable Cities Index. (2015). at <http://www.sustainablecitiesindex.com/>
3. City Vision 2050. (2015). at <http://www.cityoflondon.gov.uk/services/environment-and-planning/sustainability/transport-and-sustainability-forum/Pages/The Sustainable City Forum.aspx>
4. Vision for a sustainable Stockholm 2050. (2015). at <http://www.hallbarstad.se/projects/60-vision-for-a-sustainable-stockholm-2050>
5. 'FutureCity' Initiative. (2015). at <http://www.japanfs.org/en/projects/future_city/index.html>
6. In 2050, You Might Want To Be Living In Helsinki. (2015). at <http://www.fastcoexist.com/3039819/in-2050-you-might-want-to-be-living-in-helsinki>
7. independent from fossil fuels by 2050. (2015). at <http://denmark.dk/en/green-living/strategies-and-policies/independent-from-fossil-fuels-by-2050/>
8. Klima- og energistrategi for Oslo. (2015). at <https://www.oslo.kommune.no/politikk-og-administrasjon/miljo/oslo-kommunes-miljoarbeid/klima-og-energistrategi-for-oslo/>
9. Exciting cooperation for sustainable public transport. (2015). at <http://www.goteborgelectricity.se/en>
10. Volvo's electric hybrid buses in operation in Stockholm. (2015). at <http://news.volvogroup.com/2015/03/16/volvos-electric-hybrid-buses-in-operation-in-stockholm/>
11. Wikström, M. *Delårsrapport av Elbilsupphandlingen januari – juni 2012*. (2012).
12. Wu, G., Inderbitzin, A. & Bening, C. Total cost of ownership of electric vehicles compared to conventional vehicles: A probabilistic analysis and projection across market segments. *Energy Policy* **80,** 196–214 (2015).
13. Nykvist, B. & Nilsson, M. Rapidly falling costs of battery packs for electric vehicles. *Nat. Clim. Chang.* **5,** 100–103 (2015).
14. Rezvanizaniani, S. M., Liu, Z., Chen, Y. & Lee, J. Review and recent advances in battery health monitoring and prognostics technologies for electric vehicle (EV) safety and mobility. *J. Power Sources* **256,** 110–124 (2014).
15. USABC Energy Storage System Goals. *2015* at <http://www.uscar.org/guest/article_view.php?articles_id=85>
16. Chen, Z., Mi, C. C., Xu, J. & Member, S. Energy Management for a Power-Split Plug-in Hybrid Electric Vehicle Based on Dynamic Programming and Neural Networks. *IEEE Trans. Veh. Technol.* **63,** 1567–1580 (2014).

17. Groot, J., Swierczynski, M., Stan, A. I. & Kær, S. K. On the complex ageing characteristics of high-power LiFePO4/graphite battery cells cycled with high charge and discharge currents. *J. Power Sources* **286,** 475–487 (2015).
18. Käbitz, S., Gerschler, J. B., Ecker, M., Yurdagel, Y., Emmermacher, B., André, D., Mitsch, T. & Sauer, D. U. Cycle and Calendar Life Study of a Graphite/NMC-Based Li-Ion High Energy System Part A: Full Cell Characterization. *J. Power Sources* **239,** 572–583 (2013).
19. Lunz, B., Yan, Z., Gerschler, J. B. & Sauer, D. U. Influence of plug-in hybrid electric vehicle charging strategies on charging and battery degradation costs. *Energy Policy* **46,** 511–519 (2012).
20. Nyman, A., Zavalis, T. G., Elger, R., Behm, M. & Lindbergh, G. Analysis of the Polarization in a Li-Ion Battery Cell by Numerical Simulations. *J. Electrochem. Soc.* **157,** A1236 (2010).
21. Zhang, Y. & Harb, J. N. Performance characteristics of lithium coin cells for use in wireless sensing systems: Transient behavior during pulse discharge. *J. Power Sources* **229,** 299–307 (2013).
22. *Electrically propelled road vehicles – Test specifications for lithium-ion traction battery packs and systems – Part 1: High-power applications, ISO 12405-1*. (2011).
23. Idaho, T. & National, E. U . S . Department of Energy Vehicle Technologies Program Battery Test Manual For Plug-In Hybrid Electric Vehicles. (2008).
24. Jalkanen, K., Karppinen, J., Skogström, L., Laurila, T., Nisula, M. & Vuorilehto, K. Cycle aging of commercial NMC/graphite pouch cells at different temperatures. *Appl. Energy* **154,** 160–172 (2015).
25. Tong, S. J., Same, A., Kootstra, M. a. & Park, J. W. Off-grid photovoltaic vehicle charge using second life lithium batteries: An experimental and numerical investigation. *Appl. Energy* **104,** 740–750 (2013).
26. Zhang, C., Jiang, J., Zhang, W., Wang, Y., Sharkh, S. & Xiong, R. A Novel Data-Driven Fast Capacity Estimation of Spent Electric Vehicle Lithium-ion Batteries. *Energies* **7,** 8076–8094 (2014).
27. Vetter, J., Novák, P., Wagner, M. R., Veit, C., Möller, K. C., Besenhard, J. O., Winter, M., Wohlfahrt-Mehrens, M., Vogler, C. & Hammouche, a. Ageing mechanisms in lithium-ion batteries. *J. Power Sources* **147,** 269–281 (2005).
28. Broussely, M., Biensan, P., Bonhomme, F., Blanchard, P., Herreyre, S., Nechev, K. & Staniewicz, R. J. Main aging mechanisms in Li ion batteries. *J. Power Sources* **146,** 90–96 (2005).
29. Gering, K. L., Sazhin, S. V., Jamison, D. K., Michelbacher, C. J., Liaw, B. Y., Dubarry, M. & Cugnet, M. Investigation of path dependence in commercial lithium-ion cells chosen for plug-in hybrid vehicle duty cycle protocols. *J. Power Sources* **196,** 3395–3403 (2011).
30. Belt, J., Utgikar, V. & Bloom, I. Calendar and PHEV cycle life aging of high-energy, lithium-ion cells containing blended spinel and layered-oxide cathodes. *J. Power Sources* **196,** 10213–10221 (2011).
31. Fleischer, C., Waag, W., Bai, Z. & Sauer, D. U. On-line self-learning time forward voltage prognosis for lithium-ion batteries using adaptive neuro-

fuzzy inference system. *J. Power Sources* (2013). doi:10.1016/j.jpowsour.2013.05.114

32. Tarascon, J. M. & Armand, M. Issues and challenges facing rechargeable lithium batteries. *Nature* **414,** 359–67 (2001).
33. Zahabi, S. A. H., Miranda-Moreno, L., Barla, P. & Vincent, B. Fuel economy of hybrid-electric versus conventional gasoline vehicles in real-world conditions: A case study of cold cities in Quebec, Canada. *Transp. Res. Part D Transp. Environ.* **32,** 184–192 (2014).
34. Song, Z., Hofmann, H., Li, J., Hou, J., Han, X. & Ouyang, M. Energy management strategies comparison for electric vehicles with hybrid energy storage system. *Appl. Energy* **134,** 321–331 (2014).
35. Brown, S., Ogawa, K., Kumeuchi, Y., Enomoto, S., Uno, M., Saito, H., Sone, Y., Abraham, D. & Lindbergh, G. Cycle life evaluation of 3Ah LixMn2O4-based lithium-ion secondary cells for low-earth-orbit satellites. *J. Power Sources* **185,** 1444–1453 (2008).
36. Liaw, B. Y. & Dubarry, M. From driving cycle analysis to understanding battery performance in real-life electric hybrid vehicle operation. *J. Power Sources* **174,** 76–88 (2007).
37. Brand, M. J., Schuster, S. F., Bach, T., Fleder, E., Stelz, M., Gläser, S., Müller, J., Sextl, G. & Jossen, A. Effects of vibrations and shocks on lithium-ion cells. *J. Power Sources* **288,** 62–69 (2015).
38. Svens, P., Lindstrom, J., Gelin, O., Behm, M. & Lindbergh, G. Novel Field Test Equipment for Lithium-Ion Batteries in Hybrid Electrical Vehicle Applications. *Energies* **4,** 741–757 (2011).
39. Xing, Y., Ma, E. W. M., Tsui, K. L. & Pecht, M. Battery Management Systems in Electric and Hybrid Vehicles. *Energies* **4,** 1840–1857 (2011).
40. Weng, C., Cui, Y., Sun, J. & Peng, H. On-board state of health monitoring of lithium-ion batteries using incremental capacity analysis with support vector regression. *J. Power Sources* **235,** 36–44 (2013).
41. Dubarry, M., Bonnet, M., Dailliez, B., Teeters, A. & Liaw, B. Y. Analysis of Electric Vehicle Usage of a Hyundai Santa Fe Fleet in Hawaii. *J. Asian Electr. Veh.* **3,** 657–663 (2005).
42. Zhang, J. & Lee, J. A review on prognostics and health monitoring of Li-ion battery. *J. Power Sources* **196,** 6007–6014 (2011).
43. Pop, V., Bergveld, H. J., Notten, P. H. L. & Regtien, P. P. L. State-of-the-art of battery state-of-charge determination. *Meas. Sci. Technol.* **16,** R93–R110 (2005).
44. Plett, G. L. Extended Kalman filtering for battery management systems of LiPB-based HEV battery packs. *J. Power Sources* **134,** 277–292 (2004).
45. Plett, G. L. Extended Kalman filtering for battery management systems of LiPB-based HEV battery packs. *J. Power Sources* **134,** 252–261 (2004).
46. Plett, G. L. Extended Kalman filtering for battery management systems of LiPB-based HEV battery packs. *J. Power Sources* **134,** 262–276 (2004).
47. Sun, F., Hu, X., Zou, Y. & Li, S. Adaptive unscented Kalman filtering for state of charge estimation of a lithium-ion battery for electric vehicles. *Energy* **36,** 3531–3540 (2011).
48. Cuma, M. U. & Koroglu, T. A comprehensive review on estimation strategies used in hybrid and battery electric vehicles. *Renew. Sustain. Energy Rev.* **42,** 517–531 (2015).

49. Sun, B., Jiang, J., Zheng, F., Zhao, W., Liaw, B. Y., Ruan, H., Han, Z. & Zhang, W. Practical state of health estimation of power batteries based on Delphi method and grey relational grade analysis. *J. Power Sources* **282,** 146–157 (2015).
50. Nyman, A., Behm, M. & Lindbergh, G. Electrochemical characterisation and modelling of the mass transport phenomena in LiPF6–EC–EMC electrolyte. *Electrochim. Acta* **53,** 6356–6365 (2008).
51. Safari, M., Morcrette, M., Teyssot, a. & Delacourt, C. Life-Prediction Methods for Lithium-Ion Batteries Derived from a Fatigue Approach. *J. Electrochem. Soc.* **157,** A713 (2010).
52. Dong, T. K., Kirchev, a., Mattera, F., Kowal, J. & Bultel, Y. Dynamic Modeling of Li-Ion Batteries Using an Equivalent Electrical Circuit. *J. Electrochem. Soc.* **158,** A326 (2011).
53. Andre, D., Meiler, M., Steiner, K., Walz, H., Soczka-Guth, T. & Sauer, D. U. Characterization of high-power lithium-ion batteries by electrochemical impedance spectroscopy. II: Modelling. *J. Power Sources* **196,** 5349–5356 (2011).
54. Hu, X., Li, S. & Peng, H. A comparative study of equivalent circuit models for Li-ion batteries. *J. Power Sources* **198,** 359–367 (2012).
55. Wu, H., Yuan, S., Zhang, X., Yin, C. & Ma, X. Model parameter estimation approach based on incremental analysis for lithium-ion batteries without using open circuit voltage. *J. Power Sources* **287,** 108–118 (2015).
56. Doyle, M., Fuller, T. F. & Newman, J. Modeling of Galvanostatic Charge and Discharge of the Lithium / Polymer / Insertion Cell. *J. Electrochem. Soc.* **140,** 1526–1533 (1993).
57. Safari, M., Morcrette, M., Teyssot, A. & Delacourt, C. Life Prediction Methods for Lithium-Ion Batteries Derived from a Fatigue Approach. *J. Electrochem. Soc.* **157,** A892 (2010).
58. Dubarry, M. & Liaw, B. Y. Development of a universal modeling tool for rechargeable lithium batteries. *J. Power Sources* **174,** 856–860 (2007).
59. Eddahech, A., Briat, O., Bertrand, N., Delétage, J.-Y. & Vinassa, J.-M. Behavior and state-of-health monitoring of Li-ion batteries using impedance spectroscopy and recurrent neural networks. *Int. J. Elec. Power* **42,** 487–494 (2012).
60. Tröltzsch, U., Kanoun, O. & Tränkler, H.-R. Characterizing aging effects of lithium ion batteries by impedance spectroscopy. *Electrochim. Acta* **51,** 1664–1672 (2006).
61. Klass, V., Behm, M. & Lindbergh, G. Li-ion battery performance in electric vehicles. in *AABC 2010 - Conference Proceedings* 45–48 (2010).
62. Plug-in hybrid project PHEV, ETC Battery and FuelCells AB, Vattenfall AB, Volvo Technology AB, Volvo Personvagnar AB, financed by the Swedish Energy Agency under project number 31097-1 until 2010-12-31. (2010).
63. *Battery test manual for plug-in hybrid electric vehicles, INL/EXT-07-12536*. (2008).
64. Svens, P., Behm, M. & Lindbergh, G. Lithium-Ion Battery Cell Cycling and Usage Analysis in a Heavy-Duty Truck Field Study. *Energies* **8,** 4513–4528 (2015).

65. Cortes, C. & Vapnik, V. Support-Vector Networks. *Mach. Learn.* **20,** 273–297 (1995).
66. Hansen, T. & Wang, C.-J. Support vector based battery state of charge estimator. *J. Power Sources* **141,** 351–358 (2005).
67. Álvarez Antón, J. C., García Nieto, P. J., Blanco Viejo, C. & Vilán Vilán, J. A. Support Vector Machines Used to Estimate the Battery State of Charge. *IEEE T. Power Electr.* **28,** 5919–5926 (2013).
68. Wu, X., Mi, L., Tan, W., Qin, J. L. & Zhao, M. N. State of Charge (SOC) Estimation of Ni-MH Battery Based on Least Square Support Vector Machines. *Adv. Mat. Res.* **211-212,** 1204–1209 (2011).
69. Junping, W., Quanshi, C. & Binggang, C. Support vector machine based battery model for electric vehicles. *Energ. Convers. Manag.* **47,** 858–864 (2006).
70. Sheng, H. & Xiao, J. Electric vehicle state of charge estimation: Nonlinear correlation and fuzzy support vector machine. *J. Power Sources* **281,** 131–137 (2015).
71. Hu, J. N., Hu, J. J., Lin, H. B., Li, X. P., Jiang, C. L., Qiu, X. H. & Li, W. S. State-of-charge estimation for battery management system using optimized support vector machine for regression. *J. Power Sources* **269,** 682–693 (2014).
72. Nuhic, A., Terzimehic, T., Soczka-Guth, T., Buchholz, M. & Dietmayer, K. Health diagnosis and remaining useful life prognostics of lithium-ion batteries using data-driven methods. *J. Power Sources* **239,** 680–688 (2013).
73. Zhou, H.-X. & Qin, S. Interaction-site prediction for protein complexes: a critical assessment. *Bioinformatics* **23,** 2203–9 (2007).
74. Tay, F. E. H. & Cao, L. Application of support vector machines in financial time series forecasting. *Omega* **29,** 309–317 (2001).
75. Pai, P. & Hong, W. Forecasting regional electricity load based on recurrent support vector machines with genetic algorithms. *Electr. Power Syst. Res.* **74,** 417–425 (2005).
76. Pattipati, B., Sankavaram, C. & Pattipati, K. System Identification and Estimation Framework for Pivotal Automotive Battery Management System Characteristics. *IEEE Trans. Syst. Man, Cybern. Part C (Applications Rev.* **41,** 869–884 (2011).
77. Pattipati, B., Pattipati, K., Christopherson, J. P., Namburu, S. M., Prokhorov, D. V & Qiao, L. Automotive Battery Management Systems. 8–11 (2008).
78. Smola, A. J. & Schöllkopf, B. A tutorial on support vector regression. *Stat. Comput.* **14,** 199–222 (2004).
79. Joachims, T. *Making large-Scale SVM Learning Practical. Advances in Kernel Methods Support Vector Learning*. (MIT-Press, 1999).
80. Wang, S., Verbrugge, M., Wang, J. S. & Liu, P. Power prediction from a battery state estimator that incorporates diffusion resistance. *J. Power Sources* **214,** 399–406 (2012).
81. Weppner, W. Determination of the Kinetic Parameters of Mixed-Conducting Electrodes and Application to the System Li[sub 3]Sb. *J. Electrochem. Soc.* **124,** 1569 (1977).

82. Nyman, A., Behm, M. & Lindbergh, G. A Theoretical and Experimental Study of the Mass Transport in Gel Electrolytes I. Mathematical Analysis of Characterization Method. *J. Electrochem. Soc.* **158,** A628 (2011).
83. Yuan, S., Wu, H. & Yin, C. State of charge estimation using the extended Kalman filter for battery management systems based on the ARX battery model. *Energies* **6,** 444–470 (2013).
84. Ljung, L. *System Identification: Theory for the User*. *PTR Prentice Hall Upper Saddle River NJ* **25,** (1987).
85. Lundgren, H., Svens, P., Ekström, H., Tengstedt, C., Lindström, J., Behm, M. & Lindbergh, G. Thermal Management of Large-Format Prismatic Lithium-Ion Battery in PHEV Application. *Submitt. to J. Electrochem. Soc.* (2015).
86. Mayyas, A. R., Omar, M., Pisu, P., Al-Ahmer, A., Mayyas, A., Montes, C. & Dongri, S. Comprehensive thermal modeling of a power-split hybrid powertrain using battery cell model. *J. Power Sources* **196,** 6588–6594 (2011).
87. Klass, V., Behm, M. & Lindbergh, G. Evaluating Real-Life Performance of Lithium-Ion Battery Packs in Electric Vehicles. *ECS Trans.* **41,** 1–11 (2012).
88. Cherkassky, V. & Ma, Y. Practical selection of SVM parameters and noise estimation for SVM regression. *Neural Netw.* **17,** 113–26 (2004).
89. Nguyen, M. H. & de la Torre, F. Optimal feature selection for support vector machines. *Pattern Recognit.* **43,** 584–591 (2010).
90. Klass, V. *Data mining approaches for in-vehicle battery pack performance modelling*. (2010).
91. Zavalis, T. G., Klett, M., Kjell, M. H., Behm, M., Lindström, R. W. & Lindbergh, G. Aging in Lithium-Ion Batteries: Model and Experimental Investigation of Harvested LiFePO4 and Mesocarbon Microbead Graphite Electrodes. *Electrochim. Acta* **110,** 335–348 (2013).
92. Klett, M., Eriksson, R., Groot, J., Svens, P., Ciosek Högström, K., Lindström, R. W., Berg, H., Gustafson, T., Lindbergh, G. & Edström, K. Non-uniform aging of cycled commercial LiFePO4//graphite cylindrical cells revealed by post-mortem analysis. *J. Power Sources* **257,** 126–137 (2014).
93. Nyberg, P., Frisk, E. & Nielsen, L. Generation of equivalent driving cycles using Markov chains and mean tractive force components. in *IFAC Proceedings Volumes* 8787–8792 (2014).
94. Remmlinger, J., Buchholz, M., Meiler, M., Bernreuter, P. & Dietmayer, K. State-of-health monitoring of lithium-ion batteries in electric vehicles by on-board internal resistance estimation. *J. Power Sources* **196,** 5357–5363 (2011).
95. Wallmark, O., Nybacka, M., Malmquist, D., Wennhage, P. & Géoren, P. Design and implementation of an experimental research and concept demonstration vehicle. in *2014 IEEE Vehicle Power and Propulsion Conference* (2014).
96. Asvestopoulos, A., Frantzén, F., Gustavsson, J., Jönsson, M., Merchant, S., Sitenkov, D., Tamnakpho, J., Tideman, J., Ulke, S. & Wang, E. *Battery Management System - Research platform for predicting State-of-*

Health and State-of- Charge of electric vehicle battery packs using Support Vector Machines. (2013).